A Switched Lyapunov-Passivity Approach to Motorized FES Cycling Using Adaptive Admittance Control

Christian A. Cousin[®], Patryk Deptula[®], Courtney A. Rouse[®], and Warren E. Dixon[®], Fellow, IEEE

Abstract—For individuals with neuromuscular disorders (NDs) affecting the coordination and control of their legs, motorized functional electrical stimulation (FES) cycling serves as a rehabilitation strategy and offers numerous health benefits. A motorized FES cycle is an example of a hybrid exoskeleton involving cooperative physical human-robot interaction where both the cycle's motor and rider's muscles (through electrical stimulation) must be controlled to achieve desirable performance. A robust sliding-mode cadence controller is developed for the rider's muscles, while an adaptive admittance controller is employed on the cycle's motor to preserve rider comfort and safety. A switched systems stability analysis using Lyapunov and passivity-based methods is conducted to ensure global asymptotic stability of the admittance error system and that the cadence error system remains passive. Experiments are conducted on one able-bodied participant and four participants with NDs to illustrate the performance of the control design. For the participants with NDs, the controller achieved an average admittance tracking error of -0.08 ± 1.05 rpm at an average cadence of 47.85 ± 1.13 rpm for the desired cadence of 50 rpm.

Index Terms—Admittance, functional electrical stimulation (FES), Lyapunov, nonlinear control, rehabilitation.

I. INTRODUCTION

POR the millions of Americans physically impacted by neuromuscular disorders (NDs), such as spinal cord injury, traumatic brain injury, and stroke [1]–[3], functional electrical stimulation (FES) cycling offers a promising rehabilitation strategy. FES cycling improves various neurological, physiological, and psychological measures [4]–[6], but its metabolic efficiency is lower than volitional cycling [7] due to poor muscle control, unfavorable biomechanics, nonphysiological muscle recruitment, and other factors

Manuscript received October 4, 2020; revised February 22, 2021; accepted April 15, 2021. Date of publication May 14, 2021; date of current version February 10, 2022. Manuscript received in final form April 28, 2021. This work was supported in part by NSF under Award DGE-1842473, Award DGE-1315138, and Award 1762829. Recommended by Associate Editor Y. Pan. (Corresponding author: Christian A. Cousin.)

Christian A. Cousin is with the Department of Mechanical Engineering, The University of Alabama, Tuscaloosa, AL 35401 USA (e-mail: cacousin@eng.ua.edu).

Patryk Deptula is with The Charles Stark Draper Laboratory, Inc., Cambridge, MA 02139 USA (e-mail: pdeptula@draper.com).

Courtney A. Rouse is with the Southwest Research Institute, San Antonio, TX 78238 USA (e-mail: courtneyarouse@ufl.edu).

Warren E. Dixon is with the Department of Mechanical and Aerospace Engineering, University of Florida, Gainesville, FL 32611 USA (e-mail: wdixon@ufl.edu).

Color versions of one or more figures in this article are available at https://doi.org/10.1109/TCST.2021.3076934.

Digital Object Identifier 10.1109/TCST.2021.3076934

(see [8]–[11]). To improve the overall performance and benefits of FES-generated movements, closed-loop control of FES is warranted [12]. However, closed-loop control is challenging because the FES muscle activation dynamics are nonlinear and uncertain. Moreover, FES cycling includes a mix of continuous and discrete dynamics due to the need to switch between muscle groups in each limb [13]. Moreover, when the FES cycle is motorized, the resulting physical human–robot interaction must be carefully controlled not only to ensure user safety but to also promote rehabilitation. Safe interaction is particularly important for people with weakened or compromised functions.

While traditional control approaches, such as position and force control, have been employed on hybrid exoskeletons, an increasingly popular choice is admittance control [14], [15], developed by Hogan [16]. Because admittance control strikes a balance between position and force control, it is more concerned about behavioral regulation instead of explicit predefined trajectory tracking [17] and is commonly used in physical human–robot interaction tasks for user safety [18].

By appropriately designing an admittance controller, an assist-as-needed control paradigm is evoked, designed to assist or resist a person to accomplish some functional task [19]. Moreover, admittance control is amenable to adaptation, and numerous studies have incorporated adaptation into the inner loop position controller [19] or outer loop force feedback [20], [21]. While admittance control is traditionally viewed as a safer alternative than position/force control [14], the physical human—robot interaction can destabilize a system, and hence, a stability analysis derived control approach is motivated to provide performance guarantees.

In the context of FES cycling, traditional passivity or Lyapunov-based approaches are insufficient due to the switched system dynamics present in the system [22], [23]. To the best of our knowledge, only results such as [24]–[26] have utilized a switched systems stability analysis for FES cycling. Because admittance and cadence control are both predicated on position-based error systems, results that include cadence and admittance tracking (see [27]) can benefit from using both passivity and Lyapunov-based analyses to demonstrate the stability of the two error systems. Namely, one error system can be selected as the dominant (or convergent) system, and the other can serve as a passive system. An overview of passivity of switched systems is provided in [23] and [28].

1063-6536 © 2021 IEEE. Personal use is permitted, but republication/redistribution requires IEEE permission. See https://www.ieee.org/publications/rights/index.html for more information.

In this article, an adaptive admittance controller is developed for use on an FES cycle's electric motor, and a robust sliding-mode cadence controller is developed to stimulate the rider's muscles via FES. In addition to regulating an admittance error system, the adaptive controller is designed to compensate for the unknown nonlinear muscle control effectiveness of the rider using a neural network and for the dynamics that are able to be linearly parameterized (LP) using a gradient adaptive component. By integrating an adaptive control component through the cycle's motor to the overall control structure, the high-frequency and high-gain feedback injected through the robustifying control components can be offloaded into a feedforward signal, which decreases the system's susceptibility to noise and increases stability margins [29, p. 10]. To further motivate the use of adaptive control, the high-gain and high-frequency feedback used on the rider's muscles (which is theorized to contribute to the early onset of neuromuscular fatigue and rider discomfort) can be reduced over time and help improve tracking errors. However, as illustrated in Section II, the control effectiveness that maps input stimulation to the rider's output torque is unknown, nonlinear, and discontinuous, representing a significant challenge of adaptive control. Hence, the dynamic coupling of the controllers can be leveraged such that adaptive control is implemented through the cycle's motor, as opposed to the rider's muscles, which then shares its adaptation with the cadence controller.

Because the cycle and rider are physically coupled, the admittance and cadence controllers interact and influence each other. Both these controllers, however, utilize unique (i.e., different) position-based error systems and represent conflicting control objectives, meaning that both error systems are unable to be simultaneously driven to zero. Hence, one must be prioritized over the other and selected as the convergent error system. Because the FES cycle is designed to assist the rider in accomplishing a rehabilitation task and uses adaptive admittance control with the assist-as-needed control paradigm, it has been selected as the dominant controller or the convergent error system. Furthermore, because the FES cycle exhibits discontinuous behavior, a switched Lyapunov-passivity stability analysis for nonstrict Lyapunov-like functions [30] is provided. Through the stability analysis, the admittance error systems are shown to be globally asymptotically convergent, where the cadence error system remains passive for all time. Experimental results on four participants with NDs, including spinal cord injury, spina bifida, and Parkinson's disease, are provided to illustrate the performance of the developed controller. For the desired cadence of 50 rpm, the average admittance tracking error was -0.08 ± 1.05 rpm at an average cadence of $47.85 \pm$ 1.13 rpm, with an average max admittance error of 4.58 rpm, and an average max cadence error of 6.90 rpm. To further examine the effect of adding adaptation, comparative results using various robust/adaptive controllers are included. These results suggest that comparable results can be obtained using a robust control development as opposed to a more complex adaptive control development.

This article builds on the preliminary result in [24] and includes similar control development; however, this article

provides a refined and more complete stability analysis, including an analysis of both closed-loop error systems throughout the entire crank cycle, as opposed to [24], which limited the analysis to regions where full control authority exists. In addition, this article includes the development of a discontinuous neural network to approximate the rider's muscle control effectiveness using jump approximation functions. Moreover, the result in [24] used LaSalle-Yoshizawa corollaries developed for nonsmooth systems in [31] to establish stability, whereas this article utilizes generalized invariance-like results for switched systems [30] to prove stability. Finally, this work provides a novel stability analysis and merges a Lyapunov-based-based analysis with a passivity-based analysis to conclude overall system stability. Compared to [24], which provides results on one able-bodied participant, this work also includes a full description of the experimental testbed (i.e., the FES cycle) and experimental results on four participants with NDs.

II. DYNAMICS

The switched, nonlinear, uncertain cycle-rider dynamics are modeled as¹ [13]

$$M(q)\ddot{q} + C(q, \dot{q})\dot{q} + G(q) + P(q, \dot{q}) + b\dot{q} + d(t) = \tau_e(t) + \tau_m(q, \dot{q}, t)$$
(1)

where $q: \mathbb{R}_{\geq t_0} \to \mathcal{Q}$ denotes the measurable crank angle, the set $\mathcal{Q} \subseteq \mathbb{R}$ contains all possible crank angles, $\dot{q}: \mathbb{R}_{\geq t_0} \to \mathbb{R}$ denotes the measurable angular velocity (i.e., cadence), and $\ddot{q}: \mathbb{R}_{\geq t_0} \to \mathbb{R}$ denotes the unknown angular acceleration. The inertial, centripetal-Coriolis, and gravitational effects of the combined cycle-rider system are denoted by $M: \mathcal{Q} \to \mathbb{R}$, $C: \mathcal{Q} \times \mathbb{R} \to \mathbb{R}$, and $G: \mathcal{Q} \to \mathbb{R}$, respectively. The rider's passive viscoelastic tissue torques and the cycle's friction are denoted by $P: \mathcal{Q} \times \mathbb{R} \to \mathbb{R}$ and $b \in \mathbb{R}_{>0}$, respectively, while the system disturbances are denoted by $d: \mathbb{R}_{\geq t_0} \to \mathbb{R}$. The torque from the cycle's electric motor is denoted by $\tau_e: \mathbb{R}_{\geq t_0} \to \mathbb{R}$ and defined as

$$\tau_e(t) \triangleq B_e u_e(t) \tag{2}$$

where the known constant motor control effectiveness relating the motor's input current to output torque is denoted by $B_e \in \mathbb{R}_{>0}$, and the subsequently designed motor control current is denoted by $u_e : \mathbb{R}_{\geq t_0} \to \mathbb{R}$.

The combined torque from the rider's stimulated muscle groups is denoted by $\tau_m: \mathcal{Q} \times \mathbb{R} \times \mathbb{R}_{\geq t_0} \to \mathbb{R}$ and defined as

$$\tau_m(q, \dot{q}, t) \triangleq \sum_{m \in \mathcal{M}} b_m(q, \dot{q}) \sigma_m(q) u_h(t)$$
 (3)

where the unknown, nonlinear individual muscle control effectiveness mapping between the FES input and the muscle torque output is denoted by $b_m: \mathcal{Q} \times \mathbb{R} \to \mathbb{R}_{>0}$, and the piecewise right-continuous switching signal for activating individual muscle groups is denoted by $\sigma_m: \mathcal{Q} \to \{0, 1\}$ $\forall m \in \mathcal{M}$, where $\mathcal{M} \triangleq \{\text{RQ LQ RH LH RG LG}\}$. The set \mathcal{M} includes the right (R) and left (L) quadriceps femoris (Q),

¹For notational brevity, all explicit dependence on time, t, within the states q(t), $\dot{q}(t)$, $\ddot{q}(t)$ is suppressed.

hamstring (H), and gluteal (G) muscle groups (i.e., the stimulated muscle groups). The subsequently designed muscle control input is utilized by all muscle groups and is denoted by $u_h : \mathbb{R}_{\geq t_0} \to \mathbb{R}$. To facilitate further analysis, an unknown, nonlinear, discontinuous lumped muscle control effectiveness is denoted by $B_m : \mathcal{Q} \times \mathbb{R} \to \mathbb{R}_{>0}$ and defined as

$$B_m(q,\dot{q}) \triangleq \sum_{m \in \mathcal{M}} b_m(q,\dot{q})\sigma_m(q).$$
 (4)

The switching signal σ_m in (3) and (4) used to activate and deactivate each muscle group is defined as

$$\sigma_m(q) \triangleq \begin{cases} 1, & q \in \mathcal{Q}_m \\ 0, & q \notin \mathcal{Q}_m \end{cases}$$
 (5)

 $\forall m \in \mathcal{M}$, where $\mathcal{Q}_m \subset \mathcal{Q}$ denotes the regions in which muscle group m is able to supply a positive torque about the crank [13]. The regions are defined as $Q_m \triangleq \{q \in A\}$ $Q \mid T_m(q) \geq \delta_m \} \ \forall m \in \mathcal{M}, \text{ where } T_m : Q \rightarrow$ denotes the torque transfer ratio of each muscle group about the cycle's crank. The selectable torque transfer threshold is denoted by $\delta_m \in (0, \max(T_m(q))]$ and dictates the angles at which each muscle group is stimulated based on its respective kinematic effectiveness (i.e., its ability to transfer positive torque about the crank axis). Because the torque transfer ratios are dependent on each rider's leg geometry, they are calculated independently for each rider and based on the result in [13]. The torque transfer threshold is selected such that backpedaling is prevented, stimulation is only applied when each muscle group can positively contribute to the motion of the crank (i.e., $\delta_m > 0 \ \forall m \in \mathcal{M}$), and the onset of muscle fatigue is delayed by only stimulating muscles in kinematically efficient regions (i.e., $\tau_m(q) > \delta_m \ \forall m \in \mathcal{M}$). The union of all muscle stimulation regions establishes the FES region of the crank cycle, defined as $Q_M \triangleq \bigcup_{m \in \mathcal{M}} Q_m$, and the kinematic deadzone (KDZ) region as the remainder $Q_K \triangleq Q \setminus Q_M$. In the KDZ, $q \in \mathcal{Q}_K$, and each muscle group's torque transfer ratio is below its respective threshold (i.e., $T_m(q) < \delta_m \ \forall m \in \mathcal{M}$); therefore, no muscles are activated or receive the FES input u_h because $\sum_{m \in \mathcal{M}} \sigma_m(q) = 0$. Hence, in the KDZ, the torque generated by the rider's muscles due to stimulation is zero (i.e., $\tau_m = 0$) and has no influence on the dynamics or the subsequently defined tracking objectives.

The switching signal $\sigma_m(q) \ \forall m \in \mathcal{M}$ is discontinuous by design and discretely transitions when the measurable crank angle q is at specific known locations, e.g., when it becomes kinematically inefficient to use muscle group m to apply a positive torque about the crank. Because the position of the crank q is measurable, the switching signals are also measurable, or observable, since the torque transfer thresholds $\delta_m \ \forall m \in \mathcal{M}$ are selectable by design. As different muscles are activated through their respective switching signals, the torque input to the system discretely changes; however, the states continuously evolve. The combination of discretely changing control inputs with continuous state dynamics gives rise to a state-dependent switched system. Although the functions in (1) capture the torques affecting the dynamics of the combined cycle-rider system, the exact functions are unknown

for each rider. However, the subsequently designed controllers only require known bounds on the aforementioned functions. Specifically, the following properties are provided for the switched system in (1).

Property 1: There exist known bounding constants c_m , c_M , c_C , c_G , c_{P1} , c_{P2} , c_b , $c_d \in \mathbb{R}_{>0}$ for the dynamic functions M, C, G, P, b, and d such that $c_m \leq M \leq c_M$; $|C| \leq c_C |\dot{q}|$; $|G| \leq c_G$; $|P| \leq c_{P1} + c_{P2} |\dot{q}|$; $b \leq c_b$; and $|d| \leq c_d \ \forall t \in \mathbb{R}_{\geq t_0}$ [13], [29, p. 12], [32, p. 131], [33, p. 157], [34, p. 42].

Property 2: Parametric uncertainties within the dynamic functions M, C, G, and b are LP [29, p. 11].

Property 3: The functions \dot{M} and C satisfy $\dot{M} - 2C = 0$ [13].

Property 4: The individual muscle control effectiveness, b_m , is subject to nonlinear activation dynamics and a muscle fiber recruitment curve (commonly represented by a sigmoidal function) [35], [36]. However, when $q \in \mathcal{Q}_M$, the lumped, unknown muscle control effectiveness mapping the FES input to the output muscle force is bounded by $B_{\underline{m}} \leq B_m \leq B_{\overline{m}}$, where B_m , $B_{\overline{m}} \in \mathbb{R}_{>0}$ are known constants [37].

III. CONTROL DEVELOPMENT

In this section, two tracking objectives are presented and two controllers are developed. First, a robust sliding-mode controller is designed to activate the rider's muscles via FES for the purpose of regulating the cycle's position and cadence (i.e., the cadence controller). Second, an adaptive controller is developed (combining a neural network feedforward term to compensate for the rider's muscle control effectiveness and a gradient adaptive feedforward term to estimate the LP dynamics) to activate the cycle's motor and indirectly regulate the interaction torque between the cycle and the rider (i.e., the admittance controller). Because the admittance controller is predicated on an inner loop position controller, both the cadence and admittance controllers utilize unique position-based error systems. Accordingly, the two unique error systems are unable to simultaneously converge to zero. Consequently, the admittance error system is selected as the dominant, or convergent, error system, while the cadence error system is shown to remain passive (see Section IV). Because the two error systems are designed to be coupled, the convergence of the admittance error system directly benefits the cadence error system. A detailed overview of the control development is provided in Table I.

A. Cadence Controller

Although the rider's muscles are only active in the FES regions, the cadence error system is active $\forall t \in \mathbb{R}_{\geq t_0}$ and quantified by the tracking errors $e : \mathbb{R}_{\geq t_0} \to \mathbb{R}$ and $r : \mathbb{R}_{\geq t_0} \to \mathbb{R}$, defined as^{2,3}

$$e \triangleq q_d - q \tag{6}$$

$$r \triangleq \dot{e} + \alpha e \tag{7}$$

²For notational brevity, all functional dependencies are hereafter suppressed unless required for clarity of exposition.

³The cadence objective can be directly quantified in terms of the time derivative of the position error system, \dot{e} .

TABLE I
DETAILED CONTROL DEVELOPMENT

Subsystem	Rider	Cycle	
Objective	Cadence tracking	Admittance tracking	
Controller	Robust sliding mode	Adaptive neural network	
Actuator(s)	Leg muscles	DC motor	
Control input	Stimulation pulsewidth (μs)	Current (A)	
Stability	Passive	Asymptotic	

where $q_d: \mathbb{R}_{\geq t_0} \to \mathcal{Q}$ denotes the desired position, designed to be \mathcal{C}^2 (i.e., q_d , \dot{q}_d , $\ddot{q}_d \in \mathcal{L}_{\infty}$), and $\alpha \in \mathbb{R}_{>0}$ denotes a selectable constant control gain. The open-loop cadence error system is obtained by taking the derivative of (7), multiplying by M, adding and subtracting e, and substituting (1) and (3)–(7) to yield

$$M\dot{r} = \gamma_1 - B_m u_h - \tau_e - Cr - e \tag{8}$$

where the lumped auxiliary signal $\chi_1: \mathcal{Q} \times \mathbb{R} \times \mathbb{R}_{\geq t_0} \to \mathbb{R}$ is defined as

$$\chi_1 \triangleq M(\ddot{q}_d + \alpha r - \alpha^2 e) + C(\dot{q}_d + \alpha e) + G + P + b(\dot{q}_d - r + \alpha e) + d + e. \quad (9)$$

Using Property 1, (9) can be bounded as $|\chi_1| \le \kappa(||z||)$, where $\kappa : \mathbb{R} \to \mathbb{R}$ denotes a positive, radially unbounded, strictly increasing function, defined as

$$\kappa(\|z\|) \triangleq c_1 + c_2 \|z\| + c_3 \|z\|^2 \tag{10}$$

where $c_1, c_2, c_3 \in \mathbb{R}_{>0}$ are known constants, $\|\cdot\|$ denotes the standard Euclidean norm, and the composite error vector $z \in \mathbb{R}^2$ is defined as $z \triangleq [e\ r]^T$. Based on (8) and the subsequent stability analysis, the cadence controller is designed as

$$u_h = \frac{1}{B_m} (k_1 r + (k_2 + k_3 ||z|| + k_4 ||z||^2) \operatorname{sgn}(r))$$
 (11)

where $k_i \in \mathbb{R}_{>0} \ \forall i \in \{1, 2, 3, 4\}$ denotes constant control gains, $\operatorname{sgn}(\cdot)$ denotes the signum function, and $B_{\underline{m}}$ is introduced in Property 4. Substituting (11) into (8) yields the closed-loop cadence error system

$$M\dot{r} = \chi_1 - \tau_e - Cr - e - \frac{B_m}{B_m} \times (k_1 r + (k_2 + k_3 ||z|| + k_4 ||z||^2) \operatorname{sgn}(r)).$$
 (12)

B. Admittance Controller

While the rider's muscles are stimulated via the cadence controller to regulate the cycle's cadence, an interaction torque error is introduced, quantified by $e_{\tau}: \mathbb{R}_{\geq t_0} \to \mathbb{R}$, and defined as

$$e_{\tau} \stackrel{\triangle}{=} \tau - \tau_d$$
 (13)

where $\tau_d: \mathbb{R}_{\geq t_0} \to \mathbb{R}$ denotes the desired bounded interaction torque, and $\tau: \mathbb{R}_{\geq t_0} \to \mathbb{R}$ denotes the bounded measurable interaction torque between the cycle and rider (i.e., $\tau \in \mathcal{L}_{\infty}$)

[21], [38]. By implementing an admittance filter, the interaction torque error can be indirectly regulated and transformed into an admittance error (i.e., a modified position and cadence error), which can be directly regulated using an inner loop position controller. The admittance filter is designed as

$$e_{\tau} \triangleq M_d \ddot{q}_a + B_d \dot{q}_a \tag{14}$$

where M_d , $B_d \in \mathbb{R}_{>0}$ denote the desired inertia and damping, selected such that the transfer function of (14) is passive and q_a , \dot{q}_a , $\ddot{q}_a \in \mathcal{L}_{\infty}$ [39, p. 241, Lemma 6.4]. The terms denoted by q_a , \dot{q}_a , \ddot{q}_a : $\mathbb{R}_{\geq t_0} \to \mathbb{R}$ represent the generated admitted position, velocity, and acceleration, respectively.

To track the admitted trajectory, an adaptive inner loop position controller is designed to regulate the admittance error system, quantified by $\xi: \mathbb{R}_{\geq t_0} \to \mathbb{R}$ and $\psi: \mathbb{R}_{\geq t_0} \to \mathbb{R}$, and defined as

$$\xi \triangleq q_a + q_d - q \tag{15}$$

$$\psi \triangleq \dot{\xi} + \beta \xi \tag{16}$$

where $\beta \in \mathbb{R}_{>0}$ denotes a constant control gain. Hence, if the inner loop position controller can regulate the errors in (15) and (16), the admittance controller will emulate the admitted dynamics of the filter in (14) and accomplish its indirect torque tracking objective. The open-loop admittance error system is generated by taking the time derivative of (16), multiplying by M, and substituting (1)–(3), (15), and (16) to yield

$$M\dot{\psi} = Y\theta + d + P - C\psi - B_m u_h - B_e u_e$$

$$Y\theta \triangleq M(\ddot{q}_a + \ddot{q}_d + \beta\psi - \beta^2 \xi) + C(\dot{q}_a + \dot{q}_d + \beta\xi)$$

$$+ G + b(\dot{q}_a + \dot{q}_d - \psi + \beta\xi)$$

$$(18)$$

where $Y: \mathbb{R}^2 \times \mathbb{R}_{\geq 0} \to \mathbb{R}^{1 \times 7}$ denotes a computable regression matrix, and $\theta \in \mathbb{R}^{7 \times 1}$ denotes a matrix of constant unknown system parameters.

Remark 1: To accurately compensate for the torque introduced by the rider's muscles, it is desirable to estimate the rider's muscle control effectiveness, B_m . However, because this function is discontinuous and its parametric uncertainties are nonlinear (i.e., non-LP), it is unable to be incorporated into the regression matrix Y. Hence, a discontinuous neural network is motivated to approximate B_m . However, the functional dependencies of $B_m(q,\dot{q})$ do not exist on a compact set, and therefore, the general neural network approximation result for functions with jumps [34, p. 34, Th. 3.1.5] fails to apply without assuming the trajectories are bounded a priori. To circumnavigate this issue and facilitate the design of a discontinuous neural network, the auxiliary function $B_{m,d} \triangleq$ $B_m(q_d+q_a, \dot{q}_d+\dot{q}_a)$ is constructed. Given that q_d, \dot{q}_d, q_a , and \dot{q}_a are bounded and exist on compact sets, the general neural network approximation result for functions with jumps holds for $B_{m,d}$ and removes the restrictive requirement of a priori bounded trajectories.

Let \mathbb{S} be a compact simply connected set of \mathbb{R}^3 with the mapping $B_{m,d}: \mathbb{S} \to \mathbb{R}$. By [37] and Property 4, $B_{m,d}$ is continuous and analytic on the compact set \mathbb{S} except at known locations of discontinuities [i.e., when $\sigma_m \ \forall m \in \mathcal{M}$ transitions based on the preset muscle activation strategy in (5)]. Accordingly, based on the design of the discrete switching signals,

 $B_{m,d}$ is right-continuous with finite jumps at known locations. According to the general neural network approximation result for functions with jumps [34, p. 34, Th. 3.1.5], there then exist weights and thresholds such that the function $B_{m,d}$ can be represented by a discontinuous neural network consisting of a combination of continuous basis functions and sigmoidal jump basis functions as

$$B_{m,d}(x_d) = W_1^T \rho(V_1^T x_d) + W_2 \gamma(V_2^T x_d) + \epsilon(x_d)$$
 (19)

where $x_d \triangleq [1 \ q_d + q_a \ \dot{q}_d + \dot{q}_a]^T \in \mathbb{S}; \ V_1 \in \mathbb{R}^{3 \times L}, \ W_1 \in \mathbb{R}^{(L+1) \times 1}, \ \text{and} \ W_2 \in \mathbb{R}^{(L+1) \times 1} \ \text{are bounded unknown}$ constant ideal weight matrices of the neural network; and 2L is the number of neurons in the hidden layer of the neural network.⁴ Accordingly, the weights $V_2 \in \mathbb{R}^{3 \times L}$ are fixed and correspond to the known locations of the discontinuities⁵ in $B_{m,d}$, introduced by the switching signal σ_m .

The continuous basis function $\rho: \mathbb{R}^L \to \mathbb{R}^{L+1}$ is defined as $\rho \triangleq [1 \ \rho_1 \ \rho_2 \cdots \rho_L]^T$, where $\rho_i \ \forall i \in \{1, 2, \ldots, L\}$ represents the basis functions for L neurons, and the sigmoidal jump basis function $\gamma: \mathbb{R}^L \to \mathbb{R}^{L+1}$ is defined as $\gamma \triangleq [1 \ \gamma_1 \ \gamma_2 \cdots \gamma_L]^T$, where $\gamma_i \ \forall i \in \{1, 2, \ldots, L\}$ represents the basis functions for L neurons. The function reconstruction error is denoted by $\epsilon: \mathbb{S} \to \mathbb{R}$.

Since the weights W_1 , V_1 , and W_2 are unknown, an approximated version of (19) is

$$\hat{B}_{m,d} \triangleq \hat{W}_1^T \rho \left(\hat{V}_1^T x_d \right) + \hat{W}_2^T \gamma \left(V_2^T x_d \right) \tag{20}$$

where $\hat{V}_1: \mathbb{R}_{\geq t_0} \to \mathbb{R}^{3 \times L}$, $\hat{W}_1 \in : \mathbb{R}_{\geq t_0} \to \mathbb{R}^{(L+1) \times 1}$, and $\hat{W}_2 \in : \mathbb{R}_{\geq t_0} \to \mathbb{R}^{(L+1) \times 1}$ are the estimates of V_1 , W_1 , and W_2 , respectively. To facilitate the following development, let the notation $(\tilde{\cdot}) \triangleq (\cdot) - (\hat{\cdot})$ denote estimation errors, and let $\rho(V_1^T x_d)$ be approximated using a Taylor series expansion as

$$\rho(V_1^T x_d) = \hat{\rho} + \hat{\rho}' \tilde{V}_1^T x_d + \mathcal{O}^2$$
(21)

where $\hat{\rho} \triangleq \rho(\hat{V}_1^T x_d)$, $\hat{\rho}' \triangleq ((\partial \rho(V_1^T x_d))/(\partial V_1^T x_d))|_{\hat{V}_1^T x_d})$ denotes the partial derivative, and \mathcal{O}^2 denotes the higher order terms of the expansion.

Assumption 1: The ideal weights, thresholds, and function approximation error of (19) and higher order terms of (21) are bounded by unknown constants [32, p. 30], [34, pp. 7 and 44], [40]. This assumption is in typical NN literature although texts, such as in [34], may also assume explicit knowledge of these bounds. If the ideal weights are constrained to stay within some predefined threshold, then the function reconstruction error will be larger. Typically, this would yield a larger ultimate steady-state (SS) bound. Yet, in the current result, the mismatch resulting from limiting the magnitude of the weights is compensated through the feedback structure of the controller [40].

Returning to the open-loop admittance error system, (17) is further modified by adding and subtracting $B_{m,d}$ and ξ to yield

$$M\dot{\psi} = Y\theta + \chi_2 - \xi - C\psi - B_e u_e + Su_h - B_{m,d} u_h \tag{22}$$

where the auxiliary function $S: \mathbb{R}^2 \to \mathbb{R}$ is defined as $S \triangleq B_{m,d} - B_m$ and arises due to the mismatch introduced between B_m and $B_{m,d}$. The function S can be bounded as $|S| \le c_4$, where $c_4 \in \mathbb{R}_{>0}$ is a known constant defined as $c_4 \triangleq B_{\overline{m}} - B_{\underline{m}}$ and $B_{\overline{m}}$ and $B_{\underline{m}}$ are defined in Property 4. In (22), $\chi_2: \overline{Q} \times \mathbb{R} \times \mathbb{R}_{\geq t_0} \to \overline{\mathbb{R}}$ is defined as

$$\gamma_2 \triangleq P + \xi + d \tag{23}$$

and bounded by Property 1 as $|\chi_2| \leq c_5 + c_6 \|\phi\|$, where c_5 , $c_6 \in \mathbb{R}_{>0}$ are known constants, the vector $\phi \in \mathbb{R}^3$ is defined as $\phi \triangleq [\zeta^T \dot{q}_a]^T$, and the error $\zeta \in \mathbb{R}^2$ is defined as $\zeta \triangleq [\xi \psi]^T$.

Based on (22) and the subsequent stability analysis, the admittance controller is designed as

$$u_e = \frac{1}{B_e} (Y\hat{\theta} + k_5 \psi - \hat{B}_{m,d} u_h + (k_6 + k_7 || \phi || + k_8 |u_h|) \operatorname{sgn}(\psi))$$
(24)

where $k_i \in \mathbb{R}_{>0} \ \forall i \in \{5, 6, 7, 8\}$ denotes constant control gains, $|u_h|$ is the absolute value of the control input in (11), and $\hat{\theta}: \mathbb{R}_{\geq t_0} \to \mathbb{R}^{7 \times 1}$ denotes an estimate of the constant system parameters. In (24), the neural network term represented by $\hat{B}_{m,d}u_h$ is included to reject the rider's muscle torque by approximating the muscle control effectiveness (hence prioritizing the admittance tracking objective), and the sliding mode term is included to compensate for the disturbances injected through χ_2 and for the reconstruction error of the neural network. Substituting (24) into (22), adding and subtracting $(W_1^T \hat{\rho} + \hat{W}_1^T \hat{\rho}' \tilde{V}_1^T x_d) u_h$, utilizing (21), and performing some algebraic manipulation yields the closed-loop admittance error system

$$M\dot{\psi} = Y\tilde{\theta} - \xi - C\psi - k_5\psi - (k_6 + k_7 \|\phi\| + (k_8 + k_9 \|\zeta\|) |u_h|) \operatorname{sgn}(\psi) - (\tilde{W}_1^T \hat{\rho} + \hat{W}_1^T \hat{\rho}' \tilde{V}_1^T x_d + \tilde{W}_2^T \gamma - N) u_h + \chi_2$$
 (25)

where $\tilde{\theta}: \mathbb{R}_{\geq t_0} \to \mathbb{R}^{7 \times 1}$ denotes the error between the actual and estimated system parameters, γ is abbreviated as $\gamma = \gamma(V_2^T x_d)$, and the auxiliary function $N: \mathbb{R}^3 \to \mathbb{R}$ is defined as

$$N \triangleq S - \epsilon - \tilde{W}_1^T \hat{\rho}' \tilde{V}_1^T x_d - W_1^T \mathcal{O}^2. \tag{26}$$

By Property 4, Assumption 1, and the use of a projection algorithm, $|N| \le c_7$ for any combination of switching signals, where $c_7 \in \mathbb{R}_{>0}$ is a known constant. Based on the subsequent stability analysis, the estimates for the system parameters in (18) and the neural network weights in (20) are propagated online via the designed update laws

$$\dot{\hat{\theta}} \triangleq \operatorname{proj}(\Gamma_1 Y^T \psi) \tag{27}$$

$$\dot{\hat{W}}_1 \triangleq \operatorname{proj}(-\Gamma_2 \hat{\rho} u_h \psi) \tag{28}$$

$$\dot{\hat{V}}_1 \triangleq \operatorname{proj}(-\Gamma_3 x_d u_h \psi \hat{W}_1^T \hat{\rho}') \tag{29}$$

$$\dot{\hat{W}}_2 \triangleq \operatorname{proj}(-\Gamma_4 \gamma \, u_h \psi) \tag{30}$$

where $\Gamma_1 \in \mathbb{R}^{7 \times 7}$, $\Gamma_2 \in \mathbb{R}^{(L+1) \times (L+1)}$, $\Gamma_3 \in \mathbb{R}^{3 \times 3}$, and $\Gamma_4 \in \mathbb{R}^{(L+1) \times (L+1)}$ denote constant positive definite learning gains,

 $^{^4}$ For simplicity, the numbers of neurons in the continuous and discontinuous components of the neural network are selected equally as L but can be varied without loss of generality.

For additional details and proofs, please see [34, Secs. 3.1.2 and 3.1.3].

and $\text{proj}(\cdot)$ denotes a smooth projection algorithm [33, p. 115]. The projection algorithm for $\hat{\theta}$ is given as

$$\dot{\hat{\theta}} = \begin{cases}
\Gamma_{1}Y^{T}\psi, & \text{if } \underline{\theta} < \hat{\theta} < \overline{\theta} \\
\Gamma_{1}Y^{T}\psi, & \text{if } \hat{\theta} = \overline{\theta} \text{ and } Y^{T}\psi < 0 \\
\Gamma_{1}Y^{T}\psi, & \text{if } \hat{\theta} = \underline{\theta} \text{ and } Y^{T}\psi > 0 \\
0, & \text{if } \hat{\theta} = \overline{\theta} \text{ and } Y^{T}\psi > 0 \\
0, & \text{if } \hat{\theta} = \underline{\theta} \text{ and } Y^{T}\psi < 0
\end{cases}$$
(31)

where $\bar{\theta}, \underline{\theta} \in \mathbb{R}^{7 \times 1}$ represent known upper and lower bounds on the parametric uncertainties of M, C, G, and b by Property 1. The projection algorithms for \hat{W}_1 , \dot{V}_1 , and \dot{W}_2 are identical in structure to (31), with the upper and lower bounds conservatively selected using Assumption 1.

IV. STABILITY ANALYSIS

Both the cadence controller and admittance controller include position-based tracking errors. In the following, the issue of conflicting tracking objectives is addressed by leveraging stability results from both Lyapunov-based analysis methods and passivity methods. By design, the admittance error system is prioritized over the cadence error system. Theorem 1 provides a Lyapunov-like switched system stability analysis to illustrate global asymptotic convergence of the closed-loop admittance error system in (25) and (27)–(30). Subsequently, Theorem 2 utilizes a switched systems passivity analysis to prove that the closed-loop cadence error system is passive when admittance tracking is prioritized. Theorem 3 then merges Theorems 1 and 2 to conclude that the overall combined system yields passive behavior while simultaneously guaranteeing the admittance error $\|\zeta\| \to 0$ as $t \to \infty \ \forall t \in \mathbb{R}_{>t_0}$. To facilitate the following development, let $V_{L,1}: \mathbb{R}^{5L+11} \xrightarrow{-\infty} \mathbb{R}$ denote a positive definite candidate Lyapunov function defined as

$$V_{L,1}(\eta) \triangleq \frac{1}{2} \xi^2 + \frac{1}{2} M \psi^2 + \frac{1}{2} \tilde{\theta}^T \Gamma_1^{-1} \tilde{\theta} + \frac{1}{2} \tilde{W}_1^T \Gamma_2^{-1} \tilde{W}_1 + \frac{1}{2} \text{tr} (\tilde{V}_1^T \Gamma_3^{-1} \tilde{V}_1) + \frac{1}{2} \tilde{W}_2^T \Gamma_4^{-1} \tilde{W}_2$$
 (32)

where $\operatorname{tr}(\cdot)$ is the trace of a matrix, and $\eta: \mathbb{R}_{\geq t_0} \to \mathbb{R}^{5L+11}$ denotes a composite vector of the states of the admittance error system, defined as $\eta \triangleq [\xi \ \psi \ \tilde{\theta}^T \ \tilde{W}_1^T \ \operatorname{vec}(\tilde{V}_1^T) \ \tilde{W}_2^T]$. Note that the operator $\operatorname{vec}(\cdot)$ stacks the columns of a matrix $A \in \mathbb{R}^{m \times n}$ to form a column vector $\operatorname{vec}(A) \in \mathbb{R}^{mn}$. In addition, let $V_{L,2}: \mathbb{R}^2 \to \mathbb{R}$ denote a positive definite storage function defined as

$$V_{L,2}(z) \triangleq \frac{1}{2}Mr^2 + \frac{1}{2}e^2.$$
 (33)

Theorem 1: The admittance controller in (24) yields global asymptotic tracking in the sense that $\|\zeta\| \to 0$ as $t \to \infty$, provided that the following constant gain conditions are satisfied: $k_6 \ge c_5$, $k_7 \ge c_6$, and $k_8 \ge c_7$.

Proof: Because the closed-loop error systems in (25) and (27)–(30) are discontinuous, they do not admit classical solutions, and the following analysis will focus on the generalized solutions of (25) and (27)–(30). Using [30] as a framework, let the Filippov regularization of a

closed-loop error system be denoted by $K[\cdot]$ and the solutions of the corresponding differential inclusions (i.e., after regularization) be referred to as generalized solutions. Since (32) is continuously differentiable with respect to the states, the Clarke gradient [41] (denoted by $\partial V_{L,1}$) reduces to the standard gradient, i.e., $\partial V_{L,1}(\eta,t) = \{ [\xi M\psi \ \tilde{\theta}^T \Gamma_1^{-1} \ \tilde{W}_1^T \Gamma_2^{-1} \ \text{vec}(\tilde{V}_1^T \Gamma_3^{-1}) \ \tilde{W}_2^T \Gamma_4^{-1} \ (1/2) \dot{M} \psi^2] \}$. Using the calculus of $K[\cdot]$ from [42], a bound on the regularization of the closed-loop error systems in (25) and (27)–(30) can be computed as $G(\eta,t) \subseteq K[G(\eta,t)]$, where $G: \mathbb{R}^{5L+12} \to \mathbb{R}^{5L+12}$ is defined as $G(\eta,t) \triangleq [\dot{\xi} \dot{\psi} \ \dot{\theta}^T \ \dot{W}_1^T \ \text{vec}(\dot{V}_1)^T \ \dot{W}_2^T \ 1]^T$. Using [30, Definition 3], a bound on the generalized time derivative of the candidate Lyapunov function in (32), $\dot{V}_{L,1}$, can be computed as

$$\dot{\bar{V}}_{L,1}(\eta,t) \le \max_{p \in \partial V_{L,1}(\eta,t)} \max_{h \in K[G(\eta,t)]} p^T h. \tag{34}$$

By inserting (16) and (25) and the update laws in (27)–(30), employing Property 3, and performing cancellations, (34) can be upper bounded as

$$\dot{\bar{V}}_{L,1} \le -\beta \xi^2 - k_5 \psi^2 + |\psi \chi_2| + |\psi N| \sup(K[u_h]) - (k_6 + k_7 \|\phi\| + k_8 |u_h|) \psi K[\operatorname{sgn}](\psi)$$
 (35)

where $K[u_h] = (1/B_{\underline{m}})(k_1r + (k_2 + k_3||z|| + k_4||z||^2)K[\operatorname{sgn}](r))$. Using Property 1, (35) can be further bounded as

$$\dot{\bar{V}}_{L,1} \le -\beta \xi^2 - k_5 \psi^2 - (\lambda_1 + \lambda_2 \|\phi\| + \lambda_3 |u_h|) |\psi| \quad (36)$$

where $\sup(K[u_h]) = |u_h|$ and $\lambda_i \in \mathbb{R} \ \forall i \in \{1, 2, 3\}$ are defined as $\lambda_1 \triangleq k_6 - c_5$, $\lambda_2 \triangleq k_7 - c_6$, and $\lambda_3 \triangleq k_8 - c_7$ (where c_5 and c_6 represent the bounding constants for $|\chi_2|$, and c_7 represents the bounding constant for |N|). Provided $\lambda_1, \lambda_2, \lambda_3 \geq 0$, then the generalized time derivative in (34) can be upper bounded in both the FES and KDZ regions as

$$\dot{\bar{V}}_{L,1} \le -\beta \xi^2 - k_5 \psi^2 \tag{37}$$

 $\forall \eta \in \mathbb{R}^{5L+11}$ and for almost all $t \in \mathbb{R}_{\geq t_0}$. Hence, (32) has a common negative semidefinite derivative across both the FES and KDZ regions. This establishes the candidate Lyapunov function in (32) as a common Lyapunov function across all regions, i.e., $\forall q \in \mathcal{Q}$. By invoking [30, Th. 2] and using (32) and (37), it can be concluded that all maximal generalized solutions of the discontinuous closed-loop error systems in (25) and (27)–(30) are complete, bounded, and satisfy $|\xi|$, $|\psi|$, $||\xi|| \to 0$ as $t \to \infty$. Furthermore, since $V_{L,1} > 0$ and $\dot{V}_{L,1} \leq 0$, it follows that $V_{L,1} \in \mathcal{L}_{\infty}$. Hence, ξ , ψ , $\tilde{\theta} \in \mathcal{L}_{\infty}$, which implies that \dot{q} , $\hat{\theta} \in \mathcal{L}_{\infty}$. Since (14) is passive, q_a , \dot{q}_a , $\ddot{q}_a \in \mathcal{L}_{\infty}$, which implies that Y, $\|\phi\|$, $x_d \in \mathcal{L}_{\infty}$. By (28) and (30), and because $x_d \in \mathcal{L}_{\infty}$, then $\hat{B}_{m,d} \in \mathcal{L}_{\infty}$. Moreover, because ξ , ψ , q_a , \dot{q}_a , $\ddot{q}_a \in \mathcal{L}_{\infty}$, by (6) and (7), it can be concluded that $e, r \in \mathcal{L}_{\infty}$, and consequently $||z|| \in \mathcal{L}_{\infty}$. By (11), $u_h \in \mathcal{L}_{\infty}$, which implies that $u_e \in \mathcal{L}_{\infty}$ (i.e., both the cadence and admittance controllers are bounded). Hence, both error systems and both controllers are bounded, ensuring rider safety.

Remark 2: Although the admittance controller regulates the admittance error systems in (15) and (16), because the

admittance error systems are coupled to the cadence error systems in (6) and (7) through the relation

$$e = \xi - q_a \tag{38}$$

$$r = \psi + (\alpha - \beta)\xi - \dot{q}_a - \alpha q_a \tag{39}$$

the admittance controller is able to ensure boundedness of the cadence controller in (11) and ensure rider safety. This fact exemplifies the assist-as-needed control scheme because the admittance controller supports the cadence controller in achieving the correlated control objectives.

Theorem 2: The closed-loop cadence error system in (12) is passive from the bounded input $|\tau_e|$, to the bounded output ||z||, with the storage function $V_{L,2}$ $\forall t \in \mathbb{R}_{\geq t_0}$, provided that the following constant gain conditions are satisfied: $k_2 \geq c_1$, $k_3 \geq c_2$, and $k_4 \geq c_3$.

Proof: Similar to Theorem 1, because the closed-loop error system in (12) is discontinuous, it does not admit classical solutions, and the analysis will focus on the generalized solution of (12). To analyze the developed controller, consider the storage function defined in (33). As before, the storage function is continuously differentiable in terms of the states, and the Clarke gradient reduces to the standard gradient, i.e., $\partial V_{L,2}(z,t) = \{[e\ Mr\ (1/2)\dot{M}r^2]^T\}$. Subsequently, a bound using the regularization of the system in (12) can be computed as $F(z,t) \subseteq K[F(z,t)]$, where $F: \mathbb{R}^3 \to \mathbb{R}^3$ is defined as $F(z,t) \triangleq [\dot{e}\ \dot{r}\ 1]^T$. Using [30, Definition 3], a bound on the generalized time derivative of the storage function in (33), $V_{L,2}$, can be computed as

$$\dot{\bar{V}}_{L,2}(z,t) \le \max_{p \in \partial V_{L,2}(z,t)} \max_{h \in K[F(z,t)]} p^T h. \tag{40}$$

Using (7) and (12) and Properties 3 and 4, an upper bound for (40) can be computed for the FES region (i.e., $\forall q \in \mathcal{Q}_M$) as

$$\dot{\bar{V}}_{L,2} \le -\alpha e^2 + |r||\chi_1| - k_1 r^2 + ||z|||\tau_e|| - (k_2 + k_3 ||z|| + k_4 ||z||^2)|r|$$
(41)

 $\forall z \in \mathbb{R}^2$ and for almost all $t \in \mathbb{R}_{\geq t_0}$. Furthermore, (41) can be bounded above using Property 1 as

$$\dot{\bar{V}}_{L,2} \le -\alpha e^2 - k_1 r^2 - \lambda_5 |r| - \lambda_6 |r| ||z|| - \lambda_7 |r| ||z||^2 + ||z|| |\tau_e|$$
 (42)

where λ_5 , λ_6 , $\lambda_7 \in \mathbb{R}$ are defined as $\lambda_5 \triangleq k_2 - c_1$, $\lambda_6 \triangleq k_3 - c_2$, and $\lambda_7 \triangleq k_4 - c_3$ (where c_1 , c_2 , and c_3 represent the bounding constants for $|\chi_1|$). Provided λ_5 , λ_6 , $\lambda_7 \geq 0$, (42) can be bounded as

$$\dot{\bar{V}}_{L,2} \le -\alpha e^2 - k_1 r^2 + \|z\| |\tau_e|. \tag{43}$$

The generalized time derivative in (43) can be used with [39, Definition 6.3] to demonstrate the cadence error system is output strictly passive with input $|\tau_e|$, output ||z||, and storage function $V_{L,2} \ \forall q \in \mathcal{Q}_M$, for almost all $t \in \mathbb{R}_{>t_0}$.

When considering the KDZ region (i.e., $\forall q \in \mathcal{Q}_K$), the rider's muscles are not stimulated, and the generalized derivative of (33) is upper bounded as

$$\dot{\bar{V}}_{L,2} \le \|z\|\kappa(\|z\|) + \|z\||\tau_e| \tag{44}$$

 $\forall z \in \mathbb{R}^2$ and for almost all $t \in \mathbb{R}_{\geq t_0}$, where $\kappa(||z||)$ was defined in (10). According to [39, p. 236, Definition 6.3], the bound in (44) represents an output-feedback passive system. Although the motor is active in the KDZ region and could be used for feedback, it has been assigned to regulate the admittance error system and, therefore, is not available to close the loop on the cadence error system. However, because the closed-loop cadence error system in (12) is coupled to the closed-loop admittance error system in (25), using (38) and (39), and the result of Theorem 1, it can be shown that $\kappa(\|z\|)$ is passive with respect to τ_e . Hence, by (44), it can be concluded that the cadence error system is not only an output-feedback passive system but also the stronger result of a passive system with input $|\tau_e|$, output ||z||, and storage function $V_{L,2} \, \forall q \in \mathcal{Q}_K$. Furthermore, the result in (43) can be upper bounded by the result in (44), which ensures a common derivative and verifies (33) as a common storage function, i.e., $\forall q \in \mathcal{Q}$ [43]. By Theorem 1, u_e , $||z|| \in \mathcal{L}_{\infty}$, which, by (2) and (10), implies that τ_e , $\kappa(\|z\|) \in \mathcal{L}_{\infty}$. Hence, the closedloop cadence error system is shown to be passive with the bounded input $|\tau_e|$, bounded output ||z||, and common storage function $V_{L,2} \, \forall q \in \mathcal{Q}$. Moreover, the result in (44) can be integrated to conclude passivity $\forall t \in \mathbb{R}_{\geq t_0}$.

Theorem 3: The connection of the closed-loop cadence and admittance error systems in (12) and (25) is passive $\forall t \in \mathbb{R}_{>t_0}$.

Proof: By treating (32) as a storage function and combining it with the storage function in (33), a tertiary storage function is created for the feedback connection of the two closed-loop error systems, denoted by $V_{L,3}: \mathbb{R}^{5L+13} \to \mathbb{R}$, and defined as $V_{L,3} \triangleq V_{L,1} + V_{L,2}$. The results in (37) and (44) can then be analyzed using [39, Th. 6.1] such that $\dot{V}_{L,3} = \dot{V}_{L,1} + \dot{V}_{L,2}$, and

$$\dot{\bar{V}}_{L,3} \le \|z\|\kappa(\|z\|) + \|z\||\tau_e| - \beta\xi^2 - k_5\psi^2
\le \|z\|\kappa(\|z\|) + \|z\||\tau_e|$$
(45)

 $\forall q \in \mathcal{Q}$. Hence, by taking $V_{L,3}$ as the new storage function for the feedback connection and combining the results from Theorems 1 and 2, it can be shown that the closed-loop cadence error system in (12) is passive with input $|\tau_e|$ and output ||z||, the closed-loop admittance error systems in (25) and (27)–(29) are asymptotically regulated, and $|\xi|$, $|\psi|$, $||\xi|| \to 0$ as $t \to \infty$. Subsequently, (45) can be integrated to show that the result holds $\forall t \in \mathbb{R}_{\geq t_0}$. The feedback interconnection of the closed-loop error systems is shown in Fig. 1.

Remark 3: Theorem 1 states that the admittance controller is an asymptotically stabilizing controller for the admittance error signals ξ and ψ ; using Fig. 1 as a visual aid, the stability result can then be relaxed to state ξ and ψ are passive with respect to τ_e . Using Theorems 2 and 3 and the fact that the cadence error signals e and r are embedded in ξ , ψ , and $\|z\|$, it can be concluded that e and r are passive with respect to τ_e .

V. EXPERIMENTS

A. Experimental Testbed

The motorized FES cycle was constructed by modifying a recumbent tricycle (TerraTrike Rover) with sensors and actuators. To measure interaction torque, the original bike

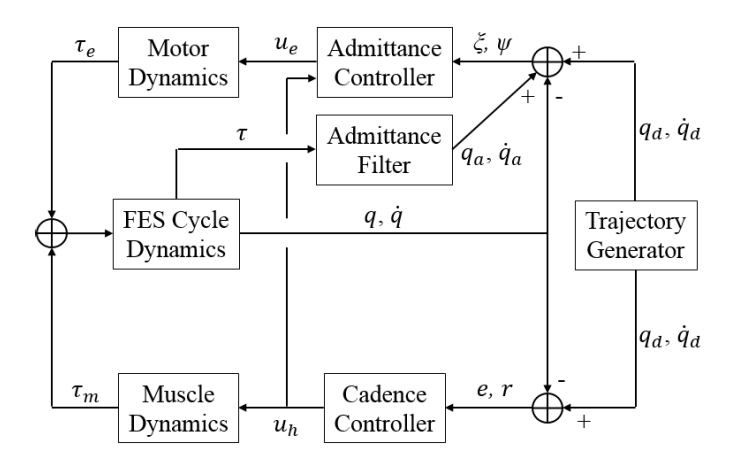


Fig. 1. Feedback interconnection of the closed-loop error systems in (12) and (25). The neural network and gradient feedforward terms, along with their corresponding updates laws, are embedded within the admittance controller block.

crank was replaced with a wireless SRM Science Road Powermeter, and to measure angular position/cadence, a US Digital H1 encoder was attached to the crank via spur gears. A 24-V, 250-W motor (Unite Motor Company Ltd., MY1016Z2) was attached to the drive chain and supplied a control current dictated by (24) through an ADVANCED Motion Controls⁶ (AMC) PS300W24 power supply and AMC AB25A100 motor driver. To reduce electrical noise on the wireless power meter, an AMC FC15030 filter card was added in-line with the motor. The rider's feet were securely attached to the cycle's pedals with modified Orthotic boots (Össur Rebound Air Tall) to maintain sagittal alignment of the legs and prevent dorsiflexion/plantarflexion of the ankles. The cycle was made stationary using a trainer and riser rings. The encoder, power meter, and motor driver were interfaced with a desktop computer running MATLAB/Simulink/Quarc through a Quanser Q-PIDe data acquisition board sampled at 500 Hz. A Hasomed Rehastim stimulator delivered symmetric, biphasic, and rectangular pulses via bipolar self-adhesive PALS⁷ electrodes to the rider's quadriceps, hamstrings, and gluteal muscle groups at respective amplitudes of 90, 80, and 70 mA at a frequency of 60 Hz. The pulsewidth was modulated automatically by the cadence controller in (11). An emergency stop button was attached to the cycle's handle to allow the rider to immediately halt the experiment. A rider seated on the motorized FES cycle is depicted in Fig. 2.

B. Experimental Methods

Experiments were conducted on one male participant with spina bifida (L5-S1, Arnold Chiari Malformation) (P1) aged 25, one female participant with a complete spinal cord injury (AIS-A, T8, and T9) (P2) aged 26, one male participant with Parkinson's disease (P3) aged 64, and one male participant with drug-induced Parkinsonism (P4) aged 57. P1 is familiar



Fig. 2. Participant 1 seated on the motorized recumbent FES cycle. Label A indicates the encoder, label B indicates the power meter, label C indicates the electrodes, label D indicates the emergency-stop, label E indicates the filter card, and label F indicates the stimulator. The electric motor is coupled to the drive chain below the seat.

with FES, regularly participates in physical and occupational therapy, uses a wheelchair part-time, and is community ambulatory with ankle-foot orthoses. P2 suffered her spinal cord injury ten years prior, uses a wheelchair full-time, and has previous experience with FES. P3 is highly active, participates in recreational activities, including swimming and boxing, and is familiar with FES. P4 had no previous exposure to FES and reported low activity levels.

To analyze the developed controllers, all participants completed two FES cycling protocols in random order: Protocol A, which enabled the controllers in (11) and (24), and Protocol B, which disabled both the neural network and adaptive feedforward components of the admittance controller in (24). By disabling adaptation, Protocol B utilized a robust admittance controller, which assumed the form

$$u_e^* = \frac{1}{B_e} (k_5 \psi + (k_6 + k_7 || \phi || + k_8 |u_h|) \operatorname{sgn}(\psi)). \tag{46}$$

To further benchmark the developed controllers in (11) and (24), two additional protocols (Protocols C and D) were run on one 28 year old able-bodied participant (P5). Protocol C disabled only the neural network component of (24) and used the admittance controller defined as

$$u_e^{\dagger} = \frac{1}{B_e} (Y \hat{\theta} + k_5 \psi + (k_6 + k_7 || \phi || + k_8 |u_h|) \operatorname{sgn}(\psi))$$
 (47)

and Protocol D disabled only the gradient adaptive component of (24) and used the admittance controller defined as

$$u_e^{\dagger} = \frac{1}{B_e} (k_5 \psi - \hat{B}_{m,d} u_h + (k_6 + k_7 || \phi || + k_8 |u_h|) \operatorname{sgn}(\psi)).$$
(48)

In addition to Protocols A and B, Protocols C and D allow for further analysis of the adaptive components of the admittance controller. The purpose of such a design was to isolate the contribution of the feedforward components of the admittance controller and determine the potentially beneficial effects of adding adaption to the FES cycle.

⁶ADVANCED Motion Controls supported the development of this testbed by providing discounts on their items.

⁷Surface electrodes for this study were provided compliments of Axelgaard Manufacturing Company Ltd.

Each protocol had a total duration of 180 s, with the first 30 s consisting of a smooth motor-only ramp to the desired cadence using (24), i.e., with the admittance controller active. While there is no clear consensus for the optimal cadence of FES cycles for rehabilitation, it has been suggested that lower cadences may be more ideal for torque production, while higher cadences may be better for power production [44]. However, without loss of generality and for feasibility purposes, the desired cadence was set to 50 rpm (as in [45] and [46]). After the initial ramp, the controller in (11) was activated, the rider was stimulated, and SS errors were recorded. Although the participants were asked to relax and not contribute to the cycling task, some volitional contribution is still possible. This contribution was not measured, and although the participants were unaware of the desired trajectories, any voluntary contribution was only partially informed by stimulation cues. To account for the electromechanical delay present in the rider's muscles, the stimulation was advanced as a function of the cadence (i.e., $q_{\text{stim}} \triangleq q + T\dot{q}$), where $q_{\text{stim}}: \mathcal{Q} \times \mathbb{R} \to \mathcal{Q}$ was substituted for q when determining σ_m , and where $T \in \mathbb{R}_{>0}$ denotes a constant estimate of the muscle delay, selected as T = 0.1 s, based on the work in [47]. For participant comfort and safety, the stimulation input u_h to the rider's muscles was individually saturated for each muscle group. The lower bound of the stimulation was set to zero, and the upper bound was determined experimentally using a series of pretests approved by the Institutional Review Boards at the University of Florida and The University of Alabama.

For all experiments, the admittance parameters in (13) and (14) were selected as $B_d = 2 [(Nm \cdot s)/rad], M_d =$ 2 [$(Nm \cdot s^2)/rad$], and $\tau_d = 0 Nm.^8$ The controller gains in (7), (11), (16), (24), and (27)–(29) were selected as $k_1 \in$ $[2, 6], k_2 = k_3 = k_4 = 0.1, k_5 = 4, k_6 = k_7 =$ $0.01, k_8 = 0.001, \alpha \in [1.0, 6.0], \beta = 0.1, \Gamma_1 =$ $\gamma \cdot \text{diag}(0.175, 0.25, 0.125, 0.5, 1.25, 1.25, 0.05), \gamma \in [1, 2],$ $\Gamma_2 = 10^{-6} \cdot \text{diag}(1.5, 1.0, 0.9, 0.75, 0.5, 2.0), \text{ and } \Gamma_3 =$ diag(0.8, 4, 0.8). For simplicity, the neural network utilized only continuous basis functions and not the discontinuous basis function component of (20); the introduced mismatch is then able to be included in the function approximation error ϵ in (19). The activation function of the neural network was selected as the soft-plus function, $\rho(V^T x) \triangleq \ln(1 +$ $\exp(V^T x)$), and the number of neurons was set to 5 (i.e., L=5). To disable each component of the controller in (24) as dictated by the protocol design, the respective learning gains (i.e., Γ_1 , Γ_2 , and Γ_3) were set to zero. To avoid transient effects from switching the admittance controller in (24) on at t = 30 s, it was enabled for all time, but the update laws were not activated until t = 30 s.

Although the aforementioned gain conditions in Theorems 1 and 2 are sufficient to achieve stability for the largest uncertainties on the system parameters, they represent the most conservative gains required by the controllers in (11) and (24). These gain conditions provided guidelines for the initial gain selection [34, p. 48], and the gains were subsequently adjusted to achieve desirable performance (e.g., the

sliding-mode gains were tuned to reduce chatter and improve rider comfort). Although the listed gains were adjusted using an empirical-based method, the gains could have been adjusted using more methodical approaches. For example, the nonlinear system in [48] was linearized at several operating points, a linear controller was designed for each point, and the gains were chosen by interpolating or scheduling the linear controllers. In [49], a neural network is used to adjust the gains of a PID controller. In [50], a genetic algorithm was used to adjust the gains after an initial guess. Killingsworth and Krstic [51] provide an extensive discussion on the use of extremum seeking for tuning the gains of a PID controller. In [34, pp. 48–49], the selection of parameters for tuning a neural network is extensively discussed, including setting the initial weights, learning gains, and selecting an appropriate number of neurons.

For this work, tuning the controllers consisted of: 1) tuning the proportional–derivative gains for desirable performance; 2) tuning the sliding-mode gains for improved performance; 3) tuning the gradient adaptive component of (24) to offload the feedback component into the feedforward component while maintaining desired performance; and 4) tuning the neural network component of (24) for further improved performance. The most sensitive parameters to tune were Γ_1 and Γ_2 . The learning gain Γ_1 was tuned element-by-element, and Γ_2 was tuned by setting all the weights inside the matrix to unique random values and then tuning a scalar multiplied against the matrix. In practice, the learning gains of the neural network should be set to unique values to allow the network to evolve using a number of rates and sensitivities.

The experimental protocols were approved by the Institutional Review Boards at the University of Florida and The University of Alabama.

C. Results and Discussion

Because the admittance controller tracks a generated admittance trajectory, and the cadence controller tracks a set cadence trajectory, the net achieved cadence is a function of the torque generated by the rider and the selected admittance parameters. Thus, if the rider is able to produce the desired amount of interaction torque (through FES), the admittance trajectory will closely align with the desired cadence trajectory, and both controllers will work in conjunction to pedal the cycle at the desired cadence. If the rider is unable to meet the desired torque (due to stimulation comfort or strength limitations), the achieved cadence will lag the desired cadence. Table II provides details on the average, maximum, and standard deviation of the measured cadence, admitted cadence, admitted cadence error, and estimated power production by the rider. The estimated power production is denoted by $\hat{\Xi}: \mathbb{R}_{\geq 0} \to \mathbb{R}$ and defined as $\hat{\Xi} \triangleq \text{mean}(\dot{q})(\text{mean}(\tau) - \tau_p)$, where τ_p : $\mathbb{R}_{>0} \to \mathbb{R}$ denotes an estimate of the passive torque required to actuate the combined rider-cycle system at the desired cadence, collected during each trial for 4.8 s prior to controller activation (i.e., approximately four crank cycles at 50 rpm). Table II also provides the average percentage of the adaptive feedforward components (comp) of the controller in (24) to the entire control effort of (24).

⁸Exceptions noted on Table III.

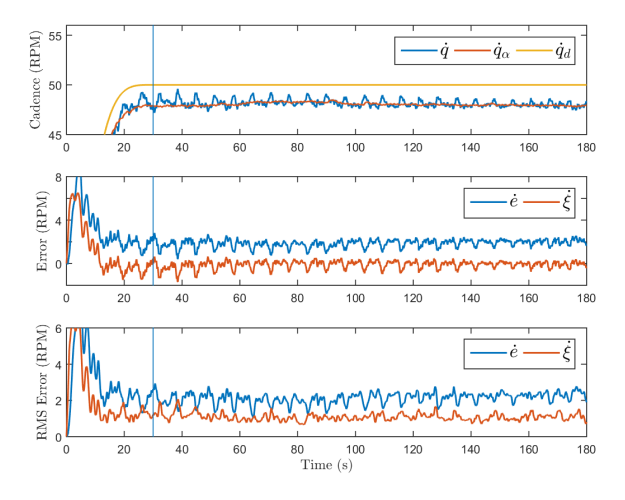


Fig. 3. P1A: (top) measured, admitted, and desired cadences; (middle) measured cadence errors; and (bottom) calculated rms cadence errors.

In the following, the participants and protocols are denoted by their respective number and letter; for example, P1 running Protocol B is referred to as P1B. Numerical results for P1–P4 are provided in Table II, calculated at steady state (i.e., after the initial cadence ramp to 50 rpm). Fig. 3 displays cadence tracking results, including errors and root-mean-squared (rms) errors for P1A; for visual clarity, a 1.2 s moving average filter was applied (i.e., approximately one crank cycle at 50 rpm). Fig. 4 displays the control inputs to both the motor and the rider's muscle groups for P1A, and for visual clarity, a 0.6 s moving average filter was applied (i.e., approximately half of a crank cycle at 50 rpm).

Prior to the cadence controller in (11) being activated, the rider's legs are assumed to produce zero torque. Hence, the rider's legs act as a drag on the system and result in a negative interaction torque. As the cycle's crank rotates, the legs effectively resist the cycle, arrest forward motion, and therefore, decrease the admitted cadence, as depicted in Fig. 3. Because only the admittance error system is being regulated at this point, the position error system (i.e., e and r) begins to accumulate; therefore, when the muscle controller in (11) is activated, a nonzero stimulation is applied, as displayed in Fig. 4. Furthermore, because the admittance controller assists the cadence controller, low values of the derivative gain were selected (i.e., $k_1 \in [2, 6]$ in the current development, compared to $k_1 \in [20, 25]$ in [13]) to avoid sharp increases in stimulation due to system disturbances and elicit a smoother stimulation pattern. The position gain (i.e., α) on the cadence error system heavily influences the stimulation increase over

Because P1 was limited in terms of his ability to generate torque from FES due to comfort thresholds, the neural network estimate of the control effectiveness relating stimulation input to torque output was near zero. However, as illustrated in Table II, adaptation results in the admittance cadence error being reduced by 11% on average, with the standard deviation of the admittance cadence error being reduced by 3%, illustrating the effect of the gradient adaptive component of the controller. It is also noted that P1 was unable to produce the desired torque; hence, his measured cadence lagged the desired

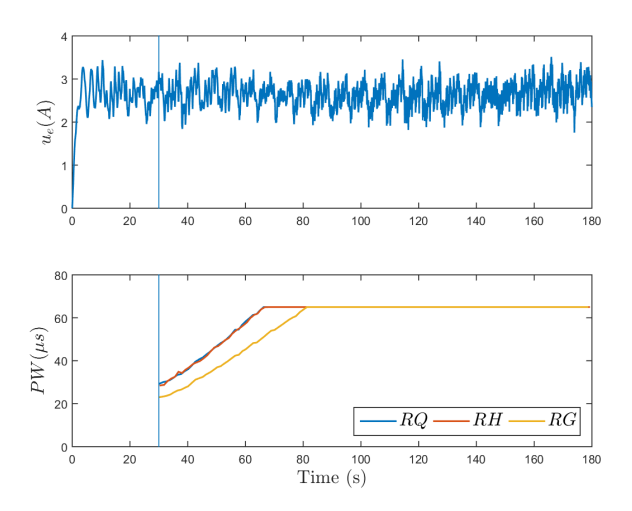


Fig. 4. P1A: (top) control input to the motor and (bottom) to the rider's quadriceps femoris, hamstrings, and gluteal muscle groups of the right leg. Due to identical muscle gains (i.e., $k_m \ \forall m \in \{Q, H\}$), the quadriceps and hamstring control inputs closely overlap. The input to the rider's muscle groups was subject to a saturation limit of 65 μ s.

for the duration of the experiment. However, the admittance error system was regulated by the admittance controller. Due to the position error accumulating, P1's stimulation steadily increased until it reached his comfort threshold, as depicted in Fig. 4. Although P1 received the maximum stimulation dictated by comfort thresholds, the cycle's cadence was held near the desired cadence because of the assistive behavior of the admittance controller. As proven by the stability analysis and indicated in Table II, the admittance error converges to near-zero values, while the cadence error remains bounded. It can be observed that the measured cadence and admitted cadence fluctuate around the desired values throughout the experiment. The cause of these fluctuations can arise from system disturbances originating from the chain links, the rider, inaccurate modeling, and so on.

Unlike P1, P2 was not limited by comfort thresholds but by significant muscle atrophy occurring in the ten years since her injury. Consequently, P2 was unable to produce much (if any) torque elicited from the applied stimulation and consequently relied exclusively on the electric motor to actuate the cycle at a near-constant cadence. Fig. 5 displays the resulting cadence and error systems for P2A. Because P2 had no sensation below the mid-abdomen, the stimulation pulsewidth was allowed to reach the hardware maximum of 500 μ s, as indicated in Fig. 6. Despite the high stimulation level, according to Table II, P2 was unable to produce any positive torque about the crank; however, P2 did get the benefit of a range-of-motion exercise on the FES cycle. Because of the lack of torque production, the neural network estimate remained at near-zero values throughout the experiment. According to Table II, using adaptation on P2 did not result in any improvement in tracking errors. Regardless, the error systems with and without adaptation remain stable in accordance with the stability analysis in Section IV.

The experimental results for P3A are depicted in Figs. 7 and 8. Unlike previous results, Fig. 7 shows that the cycle's measured cadence is above the desired cadence and does not

Participant	Protocol	$\dot{q} \; (\text{RPM})^\dagger$	\dot{q}_{α} (RPM)	$\dot{\xi}$ (RPM)	$\hat{\Xi}\left(W\right)$	$\max\left(\dot{\xi}\right)$ (RPM)	$\max(\dot{e})$ (RPM)	FF Comp. (%)
1	A	48.14±1.13	-1.95±0.21	-0.10±1.13	0.14±1.09	4.37	6.39	91.67
	В	48.14 ± 1.19	-2.04 ± 0.81	-0.19 ± 1.19	0.24 ± 1.04	7.64	9.38	0.00
2	A	47.56±0.95	-2.52±0.13	-0.08±0.95	-0.14±0.92	4.80	7.27	90.21
	В	47.48 ± 0.96	-2.57 ± 0.13	-0.05 ± 0.97	-0.15 ± 0.88	4.07	6.61	0.00
3	A	49.04±1.36	-0.94±0.77	0.01 ± 1.08	3.70±3.13	4.98	5.88	97.44
	В	48.64 ± 1.43	-1.47 ± 0.68	-0.11 ± 1.27	2.53 ± 2.67	4.17	5.94	0.00
4	A	46.66±1.04	-3.47±0.33	-0.13±1.02	-0.07±1.11	4.15	8.07	88.59
	В	47.15±0.90	-2.85 ± 0.44	0.00 ± 0.81	-0.02 ± 1.06	2.59	5.65	0.00
Mean	A	47.85±1.13	-2.22±0.43	-0.08±1.05	0.91±1.81	4.58	6.90	91.98
Mean	В	$47.85 {\pm} 1.14$	-2.23 ± 0.58	-0.09 ± 1.08	$0.65{\pm}1.59$	4.62	6.90	0.00

TABLE II
TRACKING RESULTS FOR EACH PARTICIPANT

[†]At SS, the average cadence error is calculated as $\dot{e} = 50 - \dot{q}$ (RPM).

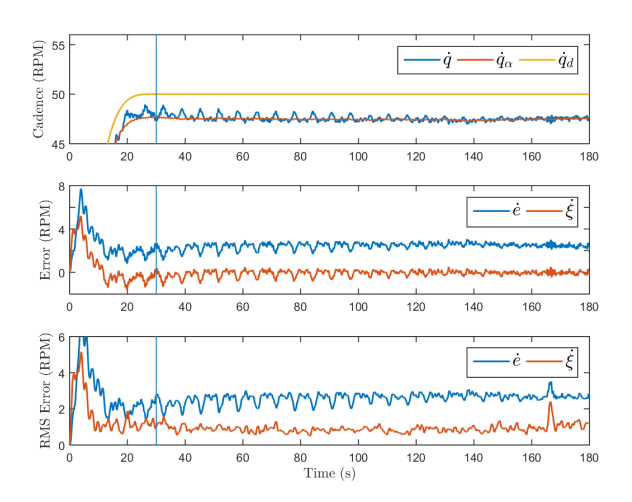


Fig. 5. P2A: (top) measured, admitted, and desired cadences; (middle) measured cadence errors; and (bottom) calculated rms cadence errors.

decrease significantly upon controller activation at t = 30 s. The stimulation pulsewidth was approximately 15 μ s at t = 30 s, as illustrated in Fig. 8. Although each participant reacts differently to the applied stimulation (hence, the uncertain nonlinear control effectiveness B_m), the authors highlight that we have not previously witnessed muscle contractions at these low stimulation levels. Consequently, we surmize that the participant was volitionally contributing to the cycling task, despite not measuring muscle activity levels with methods such as electromyography. Although the participant was blind to his performance and the desired trajectory, the applied stimulation can be used as triggering cues for the rider to pedal the cycle, and based on the stimulation intensity, with an appropriate amount of force. As the experiment progressed, however, the stimulation was observed to increase at approximately $t \approx 70$ s; at this point, we assume the rider began to relax and withdraw his volitional contributions. When the rider relaxes, the observed cadence decreases, and both error systems decrease, as shown in Fig. 7. As the experiment progresses and the stimulation is able to evoke stronger contractions, the stimulation level begins to plateau (despite

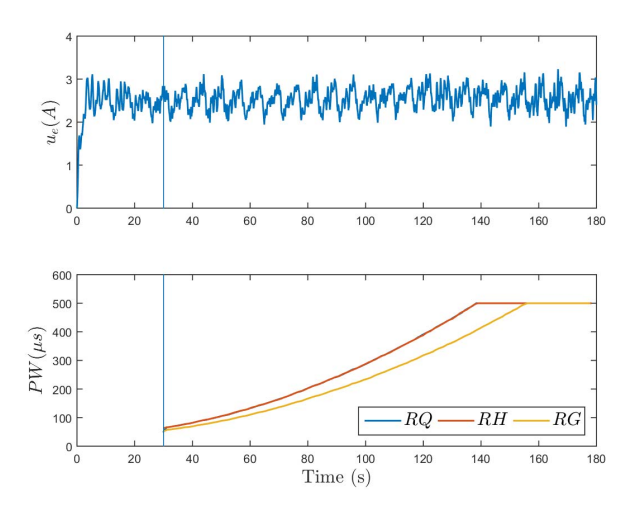


Fig. 6. P2A: (top) control input to the motor and (bottom) to the rider's quadriceps femoris, hamstrings, and gluteal muscle groups of the right leg. Due to identical muscle gains (i.e., $k_m \ \forall m \in \{Q, H\}$), the quadriceps and hamstring control inputs closely overlap. The input to the rider's muscle groups was subject to a saturation limit of 500 μ s.

saturation), indicating that the applied stimulation was nearly sufficient to evoke contractions powerful enough to pedal the cycle and overcome the passive torque required to actuate the rider's limbs. Due to the admittance filter in (14), the admitted trajectory begins to align with the desired, resulting in less error accumulation (i.e., e) and a less aggressive ramp in the stimulation input. However, as the muscles begin to fatigue, their cumulative torque production lessens, the positive interaction torque decreases, and the admitted cadence begins to decrease; consequently, the stimulation input increases to maintain torque levels. Despite the results of P3 indicating that he/she contributed to the cycling task volitionally, the adaptive admittance controller was able to reduce the admittance error to 0.01 ± 1.08 rpm compared to the nonadaptive case of -0.11 ± 1.27 rpm.

Compared to the other participants, P4's neurological condition was unique, in which his/her symptoms (i.e., tremor) were induced through oral medications and resulted in drug-induced

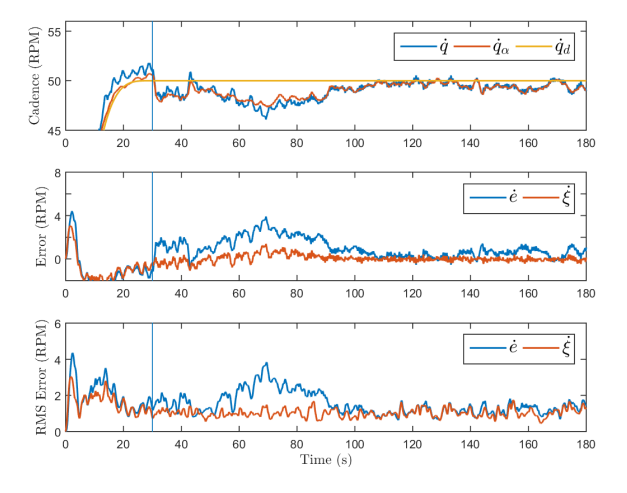


Fig. 7. P3A: (top) measured, admitted, and desired cadences; (middle) measured cadence errors; and (bottom) calculated rms cadence errors.

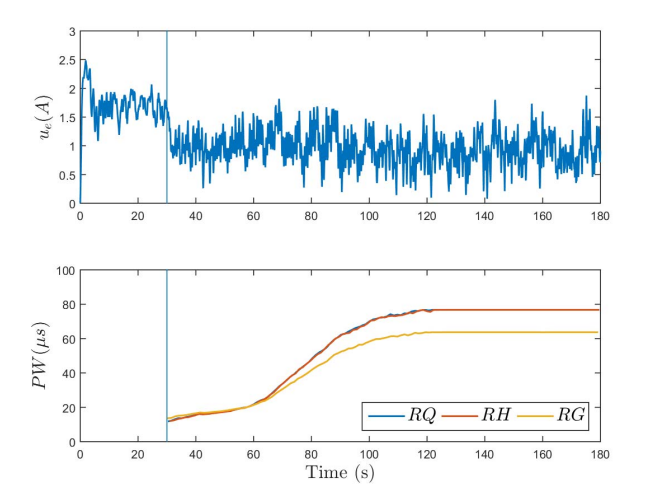


Fig. 8. P3A: (top) control input to the motor and (bottom) the rider's quadriceps femoris, hamstrings, and gluteal muscle groups of the right leg. Due to identical muscle gains (i.e., $k_m \ \forall m \in \{Q, H\}$), the quadriceps and hamstring control inputs closely overlap. The input to the rider's muscle groups was subject to a saturation limit of 77 μ s for the quadriceps and hamstrings and 63 μ s for the gluteals.

Parkinsonism. However, when P4 participated in the study, he/she had since changed medications and demonstrated no signs of discernible tremor. The results from P4A are shown in Figs. 9 and 10. Because of P4's low activity levels and sensitivity to stimulation, the applied stimulation was unable to evoke strong muscle contractions, similar to P1. Furthermore, due to participant comfort, the hamstring muscle groups were not stimulated and further limited the elicited rider torque. Of the participants with NDs, P4 was the only participant where enabling adaptation detracted from the performance of the cycle and increased the admittance error from 0.00 ± 0.81 rpm without adaptation to -0.13 ± 1.02 rpm with adaptation.

Because Protocol B disabled the adaptive component of the admittance controller and used a robust admittance controller, it was used as a quantitative benchmark. Comparing the mean tracking results from Protocol A to Protocol B lends additional insight to FES cycling and the role of adaptation. For example, although the mean admitted cadences and admitted cadence

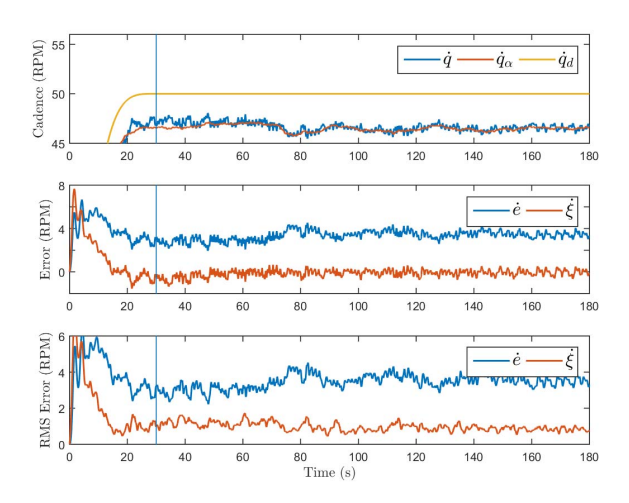


Fig. 9. P4A: (top) measured, admitted, and desired cadences; (middle) measured cadence errors; and (bottom) calculated rms cadence errors.

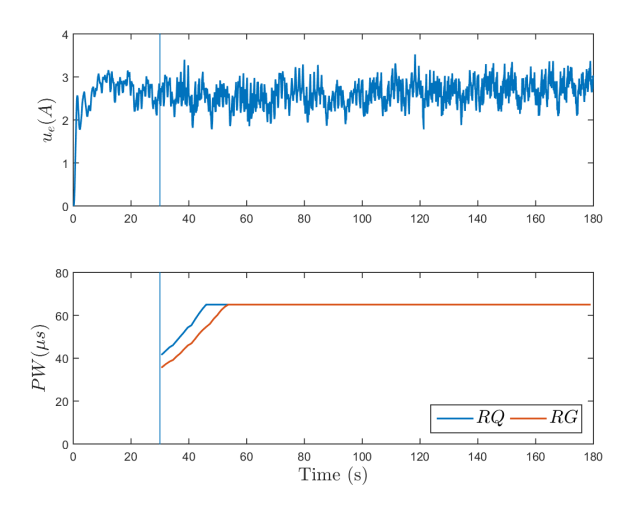


Fig. 10. P4A: (top) control input to the motor and (bottom) the rider's quadriceps femoris and gluteal muscle groups of the right leg. Due to participant comfort, the hamstring muscle groups were not stimulated. The input to the rider's muscle groups was subject to a saturation limit of 65 μ s.

errors were similar in the participants with NDs, the mean standard deviation of the admitted cadence did improve with adaptation (i.e., 0.43 rpm with adaptation, compared to 0.58 rpm without adaptation). By reducing the standard deviation of the cycle's cadence, the cycle's crank rotates more uniformly and results in a smoother and more comfortable cycling experience. Moreover, because the stimulation applied to the rider's muscles uses the cadence controller in (11), a smaller standard deviation in the cycle's cadence results in smoother stimulation patterns.

To further analyze the adaptive controller in (24), Protocols A–D were conducted on P5. Protocols A–D all used the cadence controller in (11) but varied their admittance controllers by using (24) and (46)–(48), respectively. The tracking results of these experiments are provided Table III.

As illustrated in Table III, Protocol A that utilized the controllers in (11) and (24) had the smallest standard deviation in the admittance cadence error. However, by comparing Protocols A and C (the protocols that included $Y\hat{\theta}$) to Protocols B

TABLE III
TRACKING RESULTS FOR P5

Protocol*	ė́ (RPM)	$\dot{\xi}$ (RPM)	max(ė) (RPM)	$\max\left(\dot{\xi}\right)$ (RPM)
A1	-1.75±2.16	-0.21 ± 0.53	9.32	1.90
A2	-1.60 ± 2.24	-0.20 ± 0.61	8.87	2.68
B1	-1.68 ± 2.77	-0.05 ± 0.61	10.67	2.05
B2	-1.36 ± 1.69	-0.06 ± 0.65	7.69	2.25
C1	-1.32 ± 2.37	-0.21 ± 0.64	9.48	2.97
C2	-1.31 ± 2.24	-0.22 ± 0.55	8.57	2.33
D1	-1.63 ± 2.67	-0.05 ± 0.58	9.80	2.86
D2	-0.98 ± 1.55	0.01 ± 0.85	4.66	2.68
Mean A	$-1.68{\pm}2.20$	-0.21 ± 0.57	9.09	2.29
Mean B	$-1.52{\pm}2.29$	-0.05 ± 0.63	9.18	2.15
Mean C	-1.31 ± 2.31	-0.21 ± 0.60	9.02	2.65
Mean D	$-1.30{\pm}2.18$	-0.02 ± 0.73	7.23	2.77

*Protocols which have a "1" or "2" in their title detail results for the admittance parameters $B_d=1.0~\frac{\mathrm{Nm\cdot s}}{\mathrm{rad}},~M_d=1.0,$ and $B_d=2.0~\frac{\mathrm{Nm\cdot s}}{\mathrm{rad}},~M_d=2.0,$ respectively.

and D (the protocols that excluded $Y\hat{\theta}$), it is apparent that the average admittance cadence error increased when the gradient adaptive component was included. According to Theorem 1, the adaptive admittance controller in (24) drives the admittance error system toward zero as $t \to \infty$ (i.e., asymptotically) and may be one of the reasons for the larger tracking error. Comparatively, the robust admittance controllers in Protocol B use robust high-frequency feedback to guarantee exponential convergence. While the robust controller guarantees faster convergence of the admittance error system, it is at the expense of a more aggressive control strategy (e.g., sliding mode). One of the benefits of adaptive control is the ability to offload a portion of the control input from feedback to feedforward components (as illustrated in Table II) and is one of the reasons for the lower standard deviation in the cycle's cadence. Despite the average admittance error being slightly larger, compared to the robust controller, the adaptive controller results in smoother cycling cadence at the expense of longer convergence times.

For additional analysis and benchmarking, the tracking results in Tables II and III can be compared to the results included in [25], which used robust controllers for simultaneous cadence and admittance tracking on an FES cycle (the same objective as this work). The results in [25] detail an additional 27 experiments on three able-bodied participants and four participants with NDs using four unique protocols; three protocols were conducted to examine the effect of varying the damping parameter $B_d \in \{1.0, 2.5, 5.0\}$ [(Nm·s)/rad]; and an additional protocol was conducted to examine the effects of adding rider volition. Protocol B of [25] offers the closest comparison to this work, which effectively mirrors Protocol B here (the exception being Protocol B in [25] utilized a damping parameter of $B_d = 2.5 \, [(\text{Nm} \cdot \text{s})/\text{rad}]$ compared to $B_d = 2.0$ [(Nm·s)/rad] here). For example, Cousin *et al.* [25] showed that, when using a robust admittance controller, within able-bodied participants, $\dot{\xi} = -0.05 \pm 1.52$ rpm, and within the participants with NDs, $\dot{\xi} = -0.03 \pm 0.95$ rpm. Comparatively, in this work with an adaptive admittance controller, $\dot{\xi} = -0.21 \pm 0.57$ rpm for the able-bodied participant and $\dot{\xi} = -0.08 \pm 1.05$ rpm for participants with NDs. Hence, by comparing these results, and the results shown in Tables II and III, it is not immediately apparent whether the addition of adaptation to the cycle's admittance controller lends itself to significantly improved tracking performance. Consequently, although both the robust and adaptive controllers demonstrate stable tracking performance, because the adaptive controller comes at the expense of a significantly more complex control structure, it may be more advisable to proceed with a less sophisticated robust controller, such as in [25]. Although each controller has its benefits, a robust controller may be beneficial for both the rider and the cycle's operator (e.g., study staff) due to significantly reduced tuning times and similar tracking performance.

As demonstrated by the tracking results of P1-P4, the error systems remained stable under a wide range of participant capabilities. In two participants (i.e., P1 and P3), adaptation was able to noticeably improve the tracking performance, whereas, in P4, adaptation detracted from the cycle's performance. Although the four participants reached their stimulation threshold, the position gain (i.e., α) can be reduced to increase the amount of time until saturation. Controller saturation is an undesirable obstacle in achieving accurate trajectory tracking, potentially preventing further convergence of the errors. However, from a rehabilitation perspective, saturating the muscle input may be desirable to evoke the strongest muscle contractions possible and provide the rider with a more thorough exercise regime. Recent studies, such as [52], have taken this balance into account and diverted the surplus of stimulation (i.e., the amount of stimulation above the threshold) as current to the cycle's electric motor. Regardless of the selected control strategy, balancing stimulation levels with fatigue, comfort, and torque output remains one of the foremost challenging and promising topics in FES cycling.

Although the current development represents the muscle control effectiveness only as a function of position and cadence, fatigue is an inescapable challenge of FES cycling and adds an additional layer of complexity to the control task. Across all trials, for the participants who do not quickly saturate the stimulation input, they begin to show signs of fatigue, evidenced by the increasing amount of stimulation required to complete the tracking objective (see Figs. 4 and 10). Because FES nonselectively recruits muscle fibers, closed-loop control offers one solution to compensate for the effect of fatigue. To reduce fatigue, the developed controller could have been implemented using [53], but compensating for fatigue remains an outstanding challenge in the use of FES [35]. Likewise, while results, such as in [54]-[56], offer inroads to compensating for neuromuscular delays, including such methods in more complex switched systems required for coordinating limb movements also remains an open challenge.

VI. CONCLUSION

To promote rehabilitation in individuals with NDs, the dual objectives of admittance and cadence tracking were presented

for use on an FES cycle, an example of a hybrid exoskeleton. A novel switched neuroadaptive admittance controller was implemented to activate the cycle's electric motor, while a cadence controller was implemented to activate the rider's muscles through FES. A combined switched Lyapunov-based passivity analysis for nonstrict candidate Lyapunov functions was then performed to illustrate the global asymptotic stability of the closed-loop admittance error systems and passivity of the closed-loop cadence error system. It is shown that while the cycle's motor regulates the admittance error system, it does not destabilize the cadence error system. Such a strategy allows for stable execution of physical human–robot interaction tasks, where both the human and the robot are controlled subsystems. Experiments conducted on one able-bodied participant and four participants with NDs showcase the performance of the controllers and demonstrate regulation of the admittance errors and bounded cadence errors, as proven by the stability analysis. Results suggest that comparable tracking results can be obtained using either robust or adaptive control strategies though both have their respective advantages and disadvantages. Using the developed controllers on FES cycles allows for people with NDs to perform intense, repetitive, coordinated active exercises for the purposes of rehabilitation. To further improve FES cycling as a whole, future efforts may focus on fatigue-reducing control strategies, addressing controller saturation, and investigating switched learning strategies.

ACKNOWLEDGMENT

Any opinions, findings, and conclusions or recommendations expressed in this material are those of the author(s) and do not necessarily reflect the views of the sponsoring agency. This work was done before Patryk Deptula joined The Charles Stark Draper Laboratory, Inc.

REFERENCES

- [1] S. E. Wallace and M. L. Kimbarow, *Cognitive Communication Disorders*. San Diego, CA, USA: Plural Publishing, 2016.
- [2] E. J. Benjamin et al., "Heart disease and stroke statistics-2017 update," Circulation, vol. 135, no. 10, pp. 146-603, 2017.
- [3] National Spinal Cord Injury Statistical Center, "Spinal cord injury facts and figures at a glance," J. Spinal Cord Med., vol. 37, no. 3, pp. 355–356, May 2014.
- [4] C.-W. Peng et al., "Review: Clinical benefits of functional electrical stimulation cycling exercise for subjects with central neurological impairments," J. Med. Biol. Eng., vol. 31, no. 1, pp. 1–11, 2011.
- [5] A. T. Harrington, C. G. A. McRae, and S. C. K. Lee, "Evaluation of functional electrical stimulation to assist cycling in four adolescents with spastic cerebral palsy," *Int. J. Pediatrics*, vol. 2012, pp. 1–11, 2012.
- [6] L. Griffin et al., "Functional electrical stimulation cycling improves body composition, metabolic and neural factors in persons with spinal cord injury," J. Electromyogr. Kinesiol., vol. 19, no. 4, pp. 614–622, Aug. 2009. [Online]. Available: http://www.sciencedirect.com/science/ article/pii/S1050641108000436
- [7] K. J. Hunt, D. Hosmann, M. Grob, and J. Saengsuwan, "Metabolic efficiency of volitional and electrically stimulated cycling in able-bodied subjects," *Med. Eng. Phys.*, vol. 35, no. 7, pp. 919–925, Jul. 2013.
- [8] K. J. Hunt, J. Fang, J. Saengsuwan, M. Grob, and M. Laubacher, "On the efficiency of FES cycling: A framework and systematic review," *Technol. Health Care*, vol. 20, no. 5, pp. 395–422, Sep. 2012.
- [9] M. Grohler, T. Angeli, T. Eberharter, P. Lugner, W. Mayr, and C. Hofer, "Test bed with force-measuring crank for static and dynamic investigations on cycling by means of functional electrical stimulation," *IEEE Trans. Neural Syst. Rehabil. Eng.*, vol. 9, no. 2, pp. 169–180, Jun. 2001.

- [10] R. Berkelmans, "Fes cycling," J. Autom. Control, vol. 18, no. 2, pp. 73–76, 2008.
- [11] L. D. Duffell, N. de N. Donaldson, and D. J. Newham, "Why is the metabolic efficiency of FES cycling low?" *IEEE Trans. Neural Syst. Rehabil. Eng.*, vol. 17, no. 3, pp. 263–269, Jun. 2009.
- [12] S. Jezernik, R. G. V. Wassink, and T. Keller, "Sliding mode closed-loop control of FES controlling the shank movement," *IEEE Trans. Biomed. Eng.*, vol. 51, no. 2, pp. 263–272, Feb. 2004.
- [13] M. J. Bellman, R. J. Downey, A. Parikh, and W. E. Dixon, "Automatic control of cycling induced by functional electrical stimulation with electric motor assistance," *IEEE Trans. Autom. Sci. Eng.*, vol. 14, no. 2, pp. 1225–1234, Apr. 2017.
- [14] A. J. Del-Ama, A. D. Koutsou, J. C. Moreno, A. De-Los-Reyes, A. Gil-Agudo, and J. L. Pons, "Review of hybrid exoskeletons to restore gait following spinal cord injury," *J. Rehabil. Res. Develop.*, vol. 49, no. 4, pp. 497–514, 2012.
- [15] F. Anaya, P. Thangavel, and H. Yu, "Hybrid FES-robotic gait rehabilitation technologies: A review on mechanical design, actuation, and control strategies," *Int. J. Intell. Robot. Appl.*, vol. 2, pp. 1–28, Jan. 2018.
- [16] N. Hogan, "Impedance control: An approach to manipulation: Part I—Theory," J. Dyn. Syst. Meas. Control, vol. 107, pp. 1–24, Jun. 1985.
- [17] H. Lee and N. Hogan, "Essential considerations for design and control of human-interactive robots," in *Proc. IEEE Int. Conf. Robot. Autom.* (ICRA), May 2016, pp. 3069–3074.
- [18] J. Zhang and C. C. Cheah, "Passivity and stability of human–robot interaction control for upper-limb rehabilitation robots," *IEEE Trans. Robot.*, vol. 31, no. 2, pp. 233–245, Apr. 2015.
- [19] I. Ranatunga, F. L. Lewis, D. O. Popa, and S. M. Tousif, "Adaptive admittance control for human–robot interaction using model reference design and adaptive inverse filtering," *IEEE Trans. Control Syst. Tech*nol., vol. 25, no. 1, pp. 278–285, Jan. 2017.
- [20] Y. Li, S. Sam Ge, and C. Yang, "Learning impedance control for physical robot–environment interaction," *Int. J. Control*, vol. 85, no. 2, pp. 182–193, 2012.
- [21] Y. Li and S. S. Ge, "Impedance learning for robots interacting with unknown environments," *IEEE Trans. Control Syst. Technol.*, vol. 22, no. 4, pp. 1422–1432, Jul. 2014.
- [22] D. Liberzon, *Switching in Systems and Control*. Basel, Switzerland: Birkhäuser, 2003.
- [23] J. Zhao and D. J. Hill, "Dissipativity theory for switched systems," *IEEE Trans. Autom. Control*, vol. 53, no. 4, pp. 941–953, May 2008.
- [24] C. A. Cousin, P. Deptula, C. A. Rouse, and W. E. Dixon, "Cycling with functional electrical stimulation and adaptive neural network admittance control," in *Proc. Amer. Control Conf. (ACC)*, Jul. 2019, pp. 1742–1747.
- [25] C. A. Cousin, C. A. Rouse, V. H. Duenas, and W. E. Dixon, "Controlling the cadence and admittance of a functional electrical stimulation cycle," *IEEE Trans. Neural Syst. Rehabil. Eng.*, vol. 27, no. 6, pp. 1181–1192, Jun. 2019.
- [26] C. A. Cousin et al., "Closed-loop cadence and instantaneous power control on a motorized functional electrical stimulation cycle," *IEEE Trans. Control Syst. Technol.*, vol. 28, no. 6, pp. 2276–2291, Nov. 2020.
- [27] C. A. Cousin, V. Duenas, C. Rouse, and W. E. Dixon, "Admittance control of motorized functional electrical stimulation cycle," in *Proc.* IFAC Conf. Cyber. Phys. Hum. Syst., 2018, pp. 328–333.
- [28] P. J. Antsaklis et al., "Control of cyberphysical systems using passivity and dissipativity based methods," Eur. J. Control, vol. 19, no. 5, pp. 379–388, Sep. 2013.
- [29] A. Behal, W. E. Dixon, B. Xian, and D. M. Dawson, Lyapunov-Based Control of Robotic Systems. Milton, U.K.: Taylor & Francis, 2009.
- [30] R. Kamalapurkar, J. A. Rosenfeld, A. Parikh, A. R. Teel, and W. E. Dixon, "Invariance-like results for nonautonomous switched systems," *IEEE Trans. Autom. Control*, vol. 64, no. 2, pp. 614–627, Feb. 2019.
- [31] N. Fischer, R. Kamalapurkar, and W. E. Dixon, "LaSalle-yoshizawa corollaries for nonsmooth systems," *IEEE Trans. Autom. Control*, vol. 58, no. 9, pp. 2333–2338, Sep. 2013.
- [32] F. L. Lewis, S. Jagannathan, and A. Yesildirak, Neural Network Control of Robot Manipulators and Nonlinear Systems. Philadelphia, PA, USA: CRC Press, 1998.
- [33] W. E. Dixon, A. Behal, D. M. Dawson, and S. Nagarkatti, Nonlinear Control of Engineering Systems: A Lyapunov-Based Approach. Boston, MA, USA: Birkhäuser, 2003.

- [34] F. L. Lewis, R. Selmic, and J. Campos, Neuro-Fuzzy Control of Industrial Systems with Actuator Nonlinearities. Philadelphia, PA, USA: SIAM, 2002.
- [35] D. B. Popović, "Advances in functional electrical stimulation," J. Electromyogr. Kinesiol., vol. 24, no. 6, pp. 795–802, Dec. 2014.
- [36] M. Ferrarin, F. Palazzo, R. Riener, and J. Quintern, "Model-based control of FES-induced single joint movements," *IEEE Trans. Neural Syst. Rehabil. Eng.*, vol. 9, no. 3, pp. 245–257, Sep. 2001.
- [37] N. Sharma, K. Stegath, C. M. Gregory, and W. E. Dixon, "Nonlinear neuromuscular electrical stimulation tracking control of a human limb," *IEEE Trans. Neural Syst. Rehabil. Eng.*, vol. 17, no. 6, pp. 576–584, Dec. 2009.
- [38] K. P. Tee, R. Yan, and H. Li, "Adaptive admittance control of a robot manipulator under task space constraint," in *Proc. IEEE Int. Conf. Robot. Automat.*, May 2010, pp. 5181–5186.
- [39] H. K. Khalil, Nonlinear Systems, 3rd ed. Upper Saddle River, NJ, USA: Prentice-Hall, 2002.
- [40] N. Sharma, C. M. Gregory, M. Johnson, and W. E. Dixon, "Closed-loop neural network-based NMES control for human limb tracking," *IEEE Trans. Control Syst. Technol.*, vol. 20, no. 3, pp. 712–725, May 2012.
- [41] F. H. Clarke, Optimization and Nonsmooth Analysis. Philadelphia, PA, USA: SIAM, 1990.
- [42] A. F. Filippov, "Differential equations with discontinuous right-hand side," in *Fifteen Papers on Differential Equations* (American Mathematical Society Translations), vol. 42. Providence, RI, USA: AMS, 1964, pp. 199–231.
- [43] W. M. Haddad, V. Chellaboina, and N. A. Kablar, "Non-linear impulsive dynamical systems. Part I: Stability and dissipativity," *Int. J. Control*, vol. 74, no. 17, pp. 1631–1658, 2001.
- [44] C. Fornusek and G. Davis, "Maximizing muscle force via low-cadence functional electrical stimulation cycling," *J. Rehabil. Med.*, vol. 36, no. 5, pp. 232–237, Sep. 2004.
- [45] K. J. Hunt et al., "Control strategies for integration of electric motor assist and functional electrical stimulation in paraplegic cycling: Utility for exercise testing and mobile cycling," *IEEE Trans. Neural Syst. Rehabil. Eng.*, vol. 12, no. 1, pp. 89–101, Mar. 2004.
- [46] M. O. Ibitoye, N. A. Hamzaid, N. Hasnan, A. K. Abdul Wahab, and G. M. Davis, "Strategies for rapid muscle fatigue reduction during FES exercise in individuals with spinal cord injury: A systematic review," *PLoS ONE*, vol. 11, no. 2, Feb. 2016, Art. no. e0149024.
- [47] R. J. Downey, M. Merad, E. J. Gonzalez, and W. E. Dixon, "The time-varying nature of electromechanical delay and muscle control effectiveness in response to stimulation-induced fatigue," *IEEE Trans. Neural Syst. Rehabil. Eng.*, vol. 25, no. 9, pp. 1397–1408, Sep. 2017.
- [48] N. Stefanovic, M. Ding, and L. Pavel, "An application of L₂ nonlinear control and gain scheduling to erbium doped fiber amplifiers," *Control Eng. Pract.*, vol. 15, pp. 1107–1117, Sep. 2007.
- [49] T. Fujinaka, Y. Kishida, M. Yoshioka, and S. Omatu, "Stabilization of double inverted pendulum with self-tuning neuro-PID," in *Proc. IEEE-INNS-ENNS Int. Joint Conf. Neural Netw. IJCNN Neural Comput.: New Challenges Perspect. New Millennium*, vol. 4, Jul. 2000, pp. 345–348.
- [50] F. Nagata, K. Kuribayashi, K. Kiguchi, and K. Watanabe, "Simulation of fine gain tuning using genetic algorithms for model-based robotic servo controllers," in *Proc. Int. Symp. Comput. Intell. Robot. Autom.*, Jun. 2007, pp. 196–201.
- [51] N. J. Killingsworth and M. Krstić, "PID tuning using extremum seeking: Online, model-free performance optimization," *IEEE Control Syst. Mag.*, vol. 26, no. 1, pp. 70–79, Feb. 2006.
- [52] C. A. Rouse, C. A. Cousin, B. C. Allen, and W. E. Dixon, "Split-crank cadence tracking for switched motorized FES-cycling with volitional pedaling," in *Proc. Amer. Control Conf. (ACC)*, Jul. 2019, pp. 4393–4398.
- [53] R. J. Downey, E. Ambrosini, S. Ferrante, A. Pedrocchi, W. E. Dixon, and G. Ferrigno, "Asynchronous stimulation with an electrode array reduces NMES-induced muscle fatigue during FES cycling," in *Proc. Int. Func*tion Elect. Stimul. Soc., Banff, AB, Canada, Sep. 2012, pp. 154–157.
- [54] R. Kamalapurkar, N. Fischer, S. Obuz, and W. E. Dixon, "Time-varying input and state delay compensation for uncertain nonlinear systems," *IEEE Trans. Autom. Control*, vol. 61, no. 3, pp. 834–839, Mar. 2016.
- [55] S. Obuz, R. J. Downey, J. R. Klotz, and W. E. Dixon, "Unknown time-varying input delay compensation for neuromuscular electrical stimulation," in *Proc. IEEE Conf. Control Appl. (CCA)*, Sydney, NSW, Australia, Sep. 2015, pp. 365–370.
- [56] S. Obuz, J. R. Klotz, R. Kamalapurkar, and W. Dixon, "Unknown time-varying input delay compensation for uncertain nonlinear systems," *Automatica*, vol. 76, pp. 222–229, Feb. 2017.



Christian A. Cousin received the Ph.D. degree from the Department of Mechanical and Aerospace Engineering, University of Florida, Gainesville, FL, USA, in 2019.

In 2019, he joined the Department of Mechanical Engineering, The University of Alabama, Tuscaloosa, AL, USA, as a Faculty Member. He is currently researching communication robots for law enforcement, additive friction stir deposition, and hybrid exoskeletons. His research interests include nonlinear and adaptive control, switched and

hybrid systems, cyber–physical systems, functional electrical stimulation, human–robot interaction, rehabilitation, manufacturing, robotics, and machine learning.

Dr. Cousin was awarded the National Science Foundation Graduate Research Fellowship in 2016 and the IEEE Control Systems Technology Award in 2019.



Patryk Deptula received the B.Sc. degree in mechanical engineering from Central Connecticut State University, New Britain, CT, USA, in 2014, and the Ph.D. degree in mechanical engineering from the Department of Mechanical and Aerospace Engineering, University of Florida, Gainesville, FL, USA in 2019

He performed research on the combustion of bioderived fuels in hybrid propellant rocket engines at Central Connecticut State University. He focused on reinforcement learning and adaptive control for

uncertain nonlinear systems at the University of Florida. He is currently a Senior Robotics Researcher with The Charles Stark Draper Laboratory, Inc., Cambridge, MA, USA. He has been engaged in a variety of unique and challenging projects, including the Dynetics-led NASA Artemis Human Lunar Landing System, development of GPS-denied navigation systems via celestial-object sighting techniques, and investigations into effective human—machine teaming. His research interests include, but are not limited to, data and learning-based methods; prediction, estimation, and analysis; control; sensor fusion; and robotics applied to a variety of fields.



Courtney A. Rouse received the Ph.D. degree in mechanical engineering from the University of Florida, Gainesville, FL, USA, in 2019. Her dissertation, which earned the 2020 Best Dissertation Award in Mechanical and Aerospace Engineering, focused on the control of motorized functional electrical stimulation exercises for neuromuscular therapy.

She is currently a Research Engineer with the Performance Metrology Group, Southwest Research Institute, San Antonio, TX, USA.



Warren E. Dixon (Fellow, IEEE) received the Ph.D. degree from the Department of Electrical and Computer Engineering, Clemson University, Clemson, SC, USA, in 2000.

He worked as a Research Staff Member and the Eugene P. Wigner Fellow with the Oak Ridge National Laboratory (ORNL) until 2004. He joined the Mechanical and Aerospace Engineering Department, University of Florida, where he is currently the Newton C. Ebaugh Professor and the Department Chair. His main research interests include the devel-

opment and application of Lyapunov-based control techniques for uncertain nonlinear systems.

Dr. Dixon is an ASME Fellow. From 2019 to 2020, he served as an Elected Member for the IEEE CSS BOG. His technical contributions and service to the IEEE CSS were recognized by the IEEE CSS Distinguished Member Award in 2020. From 2012 to 2015, he served as the Director of Operations for the Executive Committee of the IEEE CSS Board of Governors (BOG). From 2013 to 2018, he was an IEEE Control Systems Society (CSS) Distinguished Lecturer.